UPPSALA
UNIVERSITET

Digital Comprehensive Summaries of Uppsala Dissertations from the Faculty of Science and Technology 1485

Noise, eigenfrequencies and turbulence behavior of a 200 kW H-rotor vertical axis wind turbine

ERIK MÖLLERSTRÖM

ACTA
UNIVERSITATIS
UPSALIENSIS
UPPSALA
2017

ISSN 1651-6214
ISBN 978-91-554-9834-4
urn:nbn:se:uu:diva-316385

Dissertation presented at Uppsala University to be publicly examined in Häggsalen, Ångströmslaboratoriet, Lägerhyddsvägen 1, Uppsala, Friday, 28 April 2017 at 13:00 for the degree of Doctor of Philosophy. The examination will be conducted in English. Faculty examiner: Professor Mats Åbom (KTH Royal Institute of Technology).

Abstract
Möllerström, E. 2017. Noise, eigenfrequencies and turbulence behavior of a 200 kW H-rotor vertical axis wind turbine. *Digital Comprehensive Summaries of Uppsala Dissertations from the Faculty of Science and Technology* 1485. 89 pp. Uppsala: Acta Universitatis Upsaliensis. ISBN 978-91-554-9834-4.

Vertical-axis wind turbines (VAWTs) have with time been outrivaled by the today more common and economically feasible horizontal-axis wind turbines (HAWTs). However, VAWTs have several advantages which still make them interesting, for example, the VAWTs can have the drive train at ground level and it has been argued that they have lower noise emission. Other proposed advantages are suitability for both up-scaling and floating offshore platforms.

The work within this thesis is made in collaboration between Halmstad University and Uppsala University. A 200-kW semi-guy-wired VAWT H-rotor, owned by Uppsala University but situated in Falkenberg close to Halmstad, has been the main subject of the research although most results can be generalized to suit a typical H-rotor.

This thesis has three main topics regarding VAWTs: (1) how the wind energy extraction is influenced by turbulence, (2) aerodynamical noise generation and (3) eigenfrequencies of the semi-guy-wired tower.

The influence from turbulence on the wind energy extraction is studied by evaluating logged operational data and examining how the power curve and the tip-speed ratio for maximum Cp is impacted by turbulence. The work has showed that the T1-turbine has a good ability to extract wind energy at turbulent conditions, indicating an advantage in energy extraction at turbulent sites for VAWTs compared to HAWTs.The noise characteristics are studied experimentally, and models of the two most likely aerodynamic noise mechanisms are applied. Here, inflow-turbulence noise is deemed as the prevailing noise source rather than turbulent-boundary-layer trailing-edge noise (TBL-TE) which is the most important noise mechanism for HAWTs. The overall noise emission has also been measured and proven low compared to similar sized HAWTs.

The eigenfrequencies of a semi-guy-wired tower are also studied. Analytical expressions describing the first-mode eigenfrequency of both tower and guy wire has been derived and verified by experiments and simulations.

Keywords: VAWT, H-rotor, eigenfrequency, semi-guy-wired tower, noise emission, sound power level, microphone array, turbulence intensity, power curve

Erik Möllerström, Department of Engineering Sciences, Electricity, Box 534, Uppsala University, SE-75121 Uppsala, Sweden.

ISSN 1651-6214
ISBN 978-91-554-9834-4
urn:nbn:se:uu:diva-316385 (http://urn.kb.se/resolve?urn=urn:nbn:se:uu:diva-316385)

Tillägnad mina föräldrar
Lars & Margareta

Acknowledgement

Först och främst vill jag tacka mina handledare. Tack till min huvudhandledare Jonny Hylander för att jag fått denna chans och för att du nu hjälpt mig ta mig hela vägen till disputation! Tack till min biträdande handledare tillika rumskamrat Fredric Ottermo för all hjälp med det dagliga forskningsarbetet. Det har varit både roligt och inspirerande att jobba med dig och du har otroligt stor del i arbetet som denna avhandling består av!! Tack till Göran Sidén som med sin svårslagna erfarenhet av vindkraftsbranschen kan det mesta av det som är värt att veta i ämnet! Tack till Hans Bernhoff som har varit min länk till avdelningen i Uppsala och sett till att jag fått vara en del av forskningen som bedrivs där!

Tack till mina övriga medförfattare. Sandra Eriksson och Anders Goude för att ni delat med er av era kunskaper vilket ni gjort i betydligt fler fall än de då ni står med på författarlistan! Tack till Anders Nordborg för ett mycket intressant och givande sammarbete men ljudkamera-inspelningarna! Tack till Sebastian Larsson för roliga men iskalla ljudmätningar! Tack till Lars Bååth för hjälp med utrustning till ljudinspelningar.

Tack till Jon Kjellin och Elias Björkelund de Faire för att ni svarat på mina tekniska frågor om T1-turbinen - bra att ha någon att ringa till när man sitter inklämd högst upp i tornet och inte hittar locket till skivbromsens hydraulolja. Tack till Karl Bolin för hjälp med expertis inom ljud från vindkraft och för att du tagit dig tid när jag haft frågor!

Tack till ovan ej nämnda kollegor i ”Energigruppen” i Halmstad: Helge, Ingemar, Mei, Sven, Urban och Heidi för en trevlig arbetsmiljö samt många intressanta och lärorika diskussioner. Tack till mina forskningskamrater i ”Vindgruppen” i Uppsala: Jon, Morgan, Eduard, Stefan, Petter, Anders, Sandra, Hans, Senad, Marcus, Per, Bahri, Aya, Muhammed, Mikael och Victor!

Tack till det strategiska forskningssammarbetet STandUP for Energy för finansieringen av min doktorandanställning! Tack till Stiftelsen Olle Engkvist Byggmästare för finansiering av ljudkameramätningarna. Också tack till Ångpanneföreningens forskningsstiftelse, Bo Rydins stiftelse samt C.F. Liljewalchs stipendiestiftelse för resestipendium som gjort min doktorandtid lite mer världsomspännande!

Ett speciellt tack till mina föräldrar som lyckades hyfsat (nåja) med att uppfostra mig och lärde mig det mesta man behövde veta och inte veta här i livet samt för att ni alltid ställer upp! Tack till min storebror för att du hjälpte till och bidrog till det sistnämnda samt för att du är en bra film- och resekamrat! Tack till mina barn, helt enkelt för att ni finns! Slutligen tack till min fru Anna-Karin för att du alltid finns där för mig och barnen!

List of Papers

This thesis is based on the following papers:

I **E. Möllerström**, F. Ottermo, A. Goude, S. Eriksson, J. Hylander and H. Bernhoff. Turbulence influence on wind energy extraction for a medium size vertical axis wind turbine. *Wind Energy,* Volume 19, Pages 1963-1973, 2016.

II **E. Möllerström**, S. Eriksson, A. Goude, F. Ottermo and J. Hylander. Turbulence influence on optimum tip speed ratio for a 200 kW vertical axis wind turbine. *Journal of Physics: Conference series*, Volume 753, article no. 032048, 2016.

III **E. Möllerström**, F. Ottermo, J. Hylander and H. Bernhoff. Noise Emission of a 200 kW Vertical Axis Wind Turbine. *Energies,* Volume 9, Issue 1, 2016.

IV F. Ottermo, **E. Möllerström**, A. Nordborg, J. Hylander and H. Bernhoff. Location of aerodynamic noise sources from a 200-kW vertical-axis wind turbine. Resubmitted after revision to Journal of Sound and Vibration.

V **E. Möllerström**, F. Ottermo, J. Hylander and H. Bernhoff. Eigen frequencies of a vertical axis wind turbine tower made of laminated wood and the effect upon attaching guy wires. *Wind Engineering*, Volume 38, No 3, Pages 277-289, 2014

VI **E. Möllerström**, F. Ottermo, J. Hylander and H. Bernhoff. Avoidance of resonances in a semi-guy-wired vertical axis wind turbine. *In proceedings of EWEA 2014*. Barcelona, Spain. March 2014.

The thesis focuses on papers I-VI but also includes the peer-reviewed contribution

VII **E. Möllerström**, S. Larsson, F. Ottermo, J. Hylander and L. Bååth. Noise propagation from a vertical axis wind turbine. In *proceedings of inter.noise2014.* Melbourne, Australia. November 2014.

Reprints were made with permission from the respective publishers and are attached as appendices at the back of the printed version of this thesis. The contribution from the author to each of the papers above is described in "6. Summary of papers and author contribution", found at page 80.

Contents

Nomenclature and abbreviations

Nomenclature - Turbulence and wind energy conversion

Symbol	Unit	Quantity
B	Pa	*Air pressure*
$\widetilde{C_p}$	-	*Power coefficient from mean wind cube*
C_p	-	*Aerodynamic power coefficient*
C_T	-	*Thrust coefficient*
P_{aero}	W	*Extracted aerodynamic power*
P_{el}	W	*Generated electric power*
P_n	W	*Power normalized for standard air pressure and temperature*
P_{wind}	W	*Power in wind*
R	m	*Turbine radius*
R_0	J/(Kg K)	*Gas constant*
T_{air}	K	*Air temperature*
TI	-	*Turbulence intensity*
TKE	m^2/s^2	*Turbulence kinetic energy*
v	m/s	*Undisturbed wind speed*
$\overline{v^3}$	m^3/s^3	*Mean wind cube*
η_d	-	*Driveline efficiency*
η_g	-	*Generator efficiency*
η_m	-	*Mechanical efficiency*
$\lambda_{C_{p-max}}$	-	*Tip-speed ratio at maximum C_p*
ρ	kg/m^3	*Air density*
$\sigma_{v_{x-z}}$	m/s	*Separate standard deviations for direction x, y or z*
σ_v	m/s	*Standard deviation of wind speed for a given time period*
ω	rad/s	*Angular velocity*
λ	-	*Tip-speed ratio*

Nomenclature - Noise from vertical-axis wind turbines

Symbol	Unit	Quantity
b	dBA	*Coherent addition of sound pressure level*
c_0	m/s	*Speed of sound*
D	m	*Rotor diameter*
H	m	*Hub height*
L_p	dBA	*Sound pressure level*
$L_{p,bg}$	dBA	*Background sound pressure level (i.e. not from wind turbine)*
$L_{p,rec}$	dBA	*Recorded sound pressure level*
$L_{p,wt}$	dBA	*Sound pressure level due to wind turbine noise (noise immission)*
L_s	m	*Blade span*
L_W	dBA	*Sound power level (noise emission)*
$L_{W,wt}$	dBA	*Wind turbine sound power level*
M	-	*Blade Mach number*
P	W	*Acoustic power emitted from source*
p	Pa	*Pressure in the sound wave*
P_0	W	*Reference power used for deciding sound power level*

p_0	Pa	*Reference pressure used for deciding sound pressure level*
r_e	m	*Retarded distance between wind turbine blade and observer*
R_h	m	*Horizontal distance between tower and place of noise recording*
R_{obs}	m	*Distance between observer and tower at hub height*
S_0	m^2	*Reference area used when calculating spherical sound distribution*
V	m^3	*Volume*
v_{blade}	m/s	*Velocity of blade*
v_{loc}	m/s	*Local velocity over the airfoil*
α_{abs}	dBA/m	*The frequency dependent air absorption factor*
β	-	*Blade-azimuth (position) angle*
θ	-	*Angle between the source-observer line and the blade chord line*
φ	-	*Angle between blade plane and plane including chord direction and observer point*

Nomenclature - Eigenfrequencies of vertical-axis wind turbines

Symbol	Unit	Quantity
μ	kg/m	*Linear density*
d_{in}	m	*Inner diameter of the pipe cross-section*
d_{out}	m	*Outer diameter of the pipe cross-section*
E_t	Pa	*Elasticity modulus of tower material*
E_w	Pa	*Elasticity modulus of wire*
E_wA	N	*Axial stiffness of wire*
f	Hz	*Frequency*
$F_{1\text{-}3h}$	N	*The horizontal component of F_w of wire 1-3*
F_T	N	*Wind load acting on rotor (thrust force)*
F_w	N	*Net force from one guy wire acting on tower*
F_z	N	*Effective horizontal spring force acting on tower*
h	m	*Height of guy-wire attachment*
I	m^4	*Second moment of area*
k	N/m	*Spring constant of guy wire*
$\tilde{k}$	N/m	*Effective horizontal spring constant of guy wires*
L	m	*Length of guy wire*
m	kg	*Top mass on tower*
m_{eff}	kg	*Effective top mass*
m_{tower}	kg	*Tower mass*
n	rpm	*Rotational speed*
T	N	*Tension*
T_p	N	*Pre-tension of guy wire*
α	-	*Wire-inclination angle*
$\Delta F_{1\text{-}3h}$	N	*Addition to $F_{1\text{-}3h}$ due to tower displacement*
ΔT	N	*Tension from wind force*
ΔW	m	*Extension of wire*
ΔZ	m	*Horizontal deviation of tower at height h*

Abbreviations

FEM	Finite element method
FFT	Fast fourier transform
HAWT	Horizontal-axis wind turbine
IEC	International electrotechnical commission
rpm	Revolutions per minute
SEPA	Swedish Environmental Protection Agency
SMHI	Swedish meteorological and hydrological institute
TBL-TE noise	Turbulent-boundary-layer trailing-edge noise
TKE	Turbulence kinetic energy
VAWT	Vertical-axis wind turbine

1. Introduction

Wind turbines can be categorized by the orientation of their axis of rotation into two groups: horizontal-axis wind turbines (HAWTs) and vertical-axis wind turbines (VAWTs). From a historical perspective, different sub-concepts of both HAWTs and VAWTs have had individual threads of development in both Europe and North America. It was mainly one of these sub-concepts, the upwind 3-bladed HAWT, that established itself on the market in the 1970-80s Denmark where it thereafter has developed into the large and economically feasible wind turbines of today [1]. Today, this HAWT-type is dominating the wind turbine market and aside from corporate development it attains a vast majority of the governmental funding for wind turbine research, which continuously widens its gap to other sub-concepts. The reason for this dominance can be debated and in addition of attributes directly linked to the concept itself, the circumstances at the time of the early development were probably of importance. For example, there was a framework for stimulating market introduction and the fact that the early development focused on small, simple and robust turbines rather than the much larger, often innovative but not very reliable prototypes of the other failed HAWT and VAWT attempts [1].

However, the wind turbine industry is today facing several challenges, for example, local environmental impact as well as service cost and reliability [2-4]. These challenges match some of the possible advantages of the VAWT technology, which has led to a renewed interest in the concept. By using a vertical shaft to transfer the torque, VAWTs can have the generator and other key parts located at ground level which enables designing them with focus on performance and economy rather than size and mass. Furthermore, maintenance and modifications are made easier with these parts placed on the easily accessible tower base. Yaw motors are superfluous since VAWTs are omni-directional, which allows for a design with essentially only one moving part, including blades, struts, shaft and generator rotor which are all jointed. Additionally, the concept has shown potential for lower noise emissions, which enables establishment closer to inhabited areas [2]. Moreover, in [5] it has been shown that the concept is more suitable for up-scaling to > 10 MW than the HAWT concept and it has also been suggested that, mainly due to its low center of mass, it is more suitable for floating offshore platforms [6]. There are however several issues that only address VAWTs that needs mentioning. Of most importance, torque ripple on the long shaft and varying bending moments on the blades due to the constantly changing angle of attack makes dimensioning for fatigue more complex.

1.1 Vertical-axis wind turbines: history and present day

European style grain grinding windmills, like the ones attacked by Don Quijote, is what usually comes to mind when thinking of early-age wind power. However, even if these types of horizontal-axis windmills was introduced in Europe no later than the 12th century, the first recordings of wind turbines are from the 9th century describing Persian vertical-axis windmills [7]. Actually, vertical-axis windmills might have been in use in the Afghan highlands as early as the 7th century BC [8]. These early VAWTs where simple devices based on aerodynamic drag, the wind was simply pushing the blades of the turbine and thus creating torque. Using aerodynamic lift created by pressure difference due to the shape of the blade is far more efficient than using drag, and the first lift-based vertical-axis wind turbines were invented by Darrieus in 1925 (French patent, US patent in 1931). The Darrieus patent [9] cover both the troposkein "egg beater" shaped turbine with curved blades, sometimes referred to as Full-Darrieus turbine but commonly just Darrieus turbine (used throughout this work). The Darrieus patent also covers the straight blade H-rotor (a.k.a. Giromill). The curved blades of the Darrieus turbine are mounted directly to the rotating tower/shaft that is supported by guy wires at the top (example can be seen in Figure 1.1 and Figure 1.2) while the straight blades of the H-rotor has struts connecting them to the shaft placed inside the tower (an example of this can be seen in Figure 1.4 and Figure 1.5).

The successful development of the HAWT concept, which led to the large commercial wind turbines that are common today, is well known but simultaneously there has been lesser known attempts to develop competitive VAWTs. Although both VAWT sub-concepts have been present on both continents, the Darrieus turbine has been the main focus in North America while the H-rotor has been the sub-concept of favor in Europe. In the following chapters the most prominent of the attempts in both North America and Europe are described.

1.1.1 Darrieus turbines in North America (1970-80s)

In the 1970s, events such as the 1973 Arab oil embargo gave the United States, as well as other western countries, an incentive to look over their reliance on foreign energy sources. The Darrieus concept which since its invention in France in the 1920s had been long forgotten was reinvented by researchers at National Research Council of Canada (CNRC) in the late 1960s. In the early 1970s Sandia National Laboratories[1] was assigned to investigate alternative energy resources and quickly learned about the Canadian VAWT research which became their main focus regarding alternative energy research. Sandia developed and tested different configurations and sizes of the Darrieus turbine. Their most well-known turbine was a 2-blade (aluminum blades) variable-speed 34 m diameter, 500-kW prototype, that was coupled to an asynchronous generator by a gearbox (see Figure 1.1). This was the first curved-blade Darrieus turbine and it was designed so that most parts could

[1] Sandia National Laboratories is best known for their research within the United States nuclear weapon program regarding non-nuclear components of thermonuclear weapons.

be exchanged, thus enabling fundamental VAWT research. With the strut-free design, an impressive maximum C_p of 0.43 was reached. The turbine which was erected in 1988 was decommissioned in 1998 due to cracks appearing in its foundation [4, 10-12].

A company called The FloWind Corp utilized much of the Sandia technology to build commercial wind farms using turbines ranging up to 300-kW which initially proved to be quite reliable and efficient [4, 13]. The concept, which had its drivetrain consisting of an asynchronous generator coupled to a gearbox mounted at the tower base, initially worked well with over 500 commercial turbines operating in the mid-1980s. FloWind produced both a 2-blade fixed-speed turbine with aluminum blades (seen in Figure 1.1) and a 3-blade, dual-speed turbine with blades made out of fiberglass. The largest part of the fleet had aluminum blades which were designed to flex, which in combination with aluminum not being very endurable to cyclic stress lead to fatigue induced failures. This together with problems with funding led ultimately to FloWind going bankrupted in the mid-1990s.

Figure 1.1: Left: The 34 m 500-kW Sandia research turbine at Bushland, Texas. Photo used with permission of Sandia National Laboratories. Right: A FloWind wind farm in the mid-1980s at Cameron Ridge in the Tehachapi Pass [14]. Photo by and used with permission of Paul Gipe. All rights reserved.

In Canada, the interest in the Darrieus concept sprung from the late 1960s, continued simultaneously as the American efforts and, most often involving the earlier mentioned National Research Council of Canada (CNRC), several small- and medium sized Darrieus prototypes were erected. For example, in a CNRC collaboration, a 230-kW Darrieus turbine manufactured by the Canadian aluminum fabricator DAF Indal was erected at Iles-de-la-Madeleine in Quebec as early as 1976. DAF Indal was, although not as successful as their American competitor FloWind, present in the 1980s California market with commercial production of Darrieus turbines [12].

All discussions on North American VAWT history eventually ends up at the record-breaking Darrieus turbine ÉOLE (French for Aeolus, the ruler of wind in Greek mythology) which was inaugurated in 1987 in Cap-Chat, Quebec, and was

with a total height of 110 m, rotating mass of 880 metric tons and rated power of 3.8 MW by far the largest VAWT ever constructed [10, 13, 15]. It was initiated by CNRC and the province-owned electric utility company Hydro-Québec with several other research institutes and companies involved. Unlike the gearbox-equipped Sandia and FloWind turbines it had a direct driven asynchronous generator based at ground level which with the help of a DC/AC-converter enabled variable speed of the 2-bladed (steel-core blades) construction [10]. Due to fatigue life predictions, the rotational speed and cut-out wind speed was limited which in reality gave a maximum power of around 2 MW [10]. It was shut down in 1993 due to failure of the bottom bearing but is kept intact and serves as a popular tourist attraction with guided tours during summers.

Figure 1.2: The 3.8 MW ÉOLE turbine at Cap-Chat, Quebec. Photos taken during a guided tour in 2016 at which time the turbine had been standing still for 23 years.

Although it is difficult to point out a single reason why the North American Darrieus efforts failed, it is probably best explained as a combination of fatigue problems with many of the turbines, drawbacks in renewable energy research funding during the 1980s and the fact that the by that time relative cost-effective and reliable European manufactured HAWTs were made available on the North American market during the 1990s.

1.1.2 H-rotors in Europe (1980-90s)

Partially overlapping with the North American Darrieus development, VAWTs were also investigated in Europe, but on this side of the Atlantic Ocean most focus was put on the H-rotor concept [4, 13, 16, 17]. The H-rotor has some advantages compared to the conventional Darrieus turbine. It is usually placed on a higher tower which both gives better energy yield and enables keeping the rotor above the surface-layer turbulence, thus avoiding the wear associated with it. Additionally, the straight blades makes it more simple and cheap to manufacture and since guy wires are not needed, the land use is smaller. There are off course drawbacks as well, the bending moments on the blades are larger and the necessity of struts makes aerodynamic and noise optimization more complex [4, 10].

Culminating in the 1980s and early 1990s, the H-rotor was investigated in a British effort led by Peter Musgrove at the University of Reading, which 2-blade concept had a gearbox coupled to an asynchronous generator. The most notable prototypes were a 130-kW variable-geometry variable-speed turbine (erected in 1986) which could feather the blades to regulate power and a 500-kW fixed-blade stall-regulated dual-speed turbine (erected in 1990), both located in Carmarthen Bay in Wales (both seen in Figure 1.3). The 130-kW turbine had the drivetrain (gearbox and generator) placed at ground level while for the succeeding 500-kW turbine, the shaft (as well as the variable geometry) was deemed as a weak point and thus the drivetrain was, similar to a HAWT, placed at the top of the tower. The latter had several failures linked to the power transmission and ultimately a devastating failure of either the main bearing or one of the fiberglass blades[2]. Both turbines were demolished around year 2000.

Figure 1.3: Left: The 130-kW Musgrove variable-geometry H-rotor (known as the VAWT-450) with the blades reefed (the blades were straight at maximum power mode). Photo by, and used with permission of, Jos Beurskens. Right: The 500-kW Musgrove H-rotor (known as VAWT-850) as featured on the front cover of Modern Power Systems in the 1990 October issue. Used with permission of Modern Power Systems.

In the 1990s the German company Heidelberg Motor GmbH developed a variable-speed H-rotor concept with direct driven permanent-magnet generators placed on top of the tower [1, 10, 18, 19]. Most prominently, they built five 2-bladed 300-kW turbines in Kaiser-Wilhelm-Koog on the German North Sea coastline (seen in in Figure 1.4). A welding problem at a rotor head in one of the turbines led to an operation halt of all five turbines by the certification body and ultimately the

[2] In [13] it is stated that the final failure was that of the main bearing while in [4, 17] it is stated that it was a blade failure due to a manufacturing defect.

turbines were dismantled in 1997. Their smaller 3-bladed 20-kW extreme-environment model was installed at Mt. Karisimbi in Rwanda, at the Mangfall Mountains in the German Alps and the German Neumayer-Station II research facility in Antarctica. The latter was in operation for more than 15 years before decommissioned with the station (that was replaced with the Neumayer-Station III) in 2008.

Figure 1.4: Left: Heidelberg 300-kW H-rotors in Kaiser-Wilhelm-Koog. Photo by and used with permission of Jörg Bendfeld. Right: Heidelberg 20-kW at the Neumayer-Station II in Antarctica [20]. Photo by and used with permission of Saad El Naggar.

In addition to the earlier mentioned competition from the by the 1990s successful HAWT concept, these H-rotor projects probably failed to achieve commercial success due to a combination of problems with durability and difficulties to get renewed governmental funding [13]. Although the Heidelberg concept was quite sophisticated with a direct driven permanent-magnet generator and variable speed, it as well as the Musgrove concept missed out on one of the main advantages of VAWTs – having an easy accessible ground based drivetrain designed for cost-efficiency and performance rather than size. Also, both Musgrove and Heidelberg concepts were 2-bladed which meant it had to cope with cyclic torque which may have added to structural difficulties.

1.1.3 The 200-kW T1-turbine

The company Vertical Wind AB[3] started working with H-rotors with the aim to produce competitive commercial turbines by capitalizing on the simplicity and robustness that should be possible for VAWTs. The main idea was to have as few moving parts as possible, this by using the electrical system rather than mechanical solutions for controlling the turbine operation. Also, the direct driven generator that is designed for the specific turbine speed and torque is kept at ground level (which

[3] A spinoff company from the Division of Electricity at Uppsala University.

then can be designed with focus on cost and efficiency rather than mass and size). Another advantage is that the direct driven concept eliminates the need for a gearbox, which according to a study of wind turbine failures in Sweden, Finland and Germany during 1997-2005 is the most critical component regarding downtime per failure [21]. Other components associated with downtime such as the yaw and pitch systems is also made superfluous for the specific concept.

The first step was to produce turbines in the 200-kW segment and thereafter move on to multi-MW turbines. However, the initiative was halted when a key financier dropped off, at a stage when only one of the planned four 200-kW prototypes were finished, thus preventing the implementation of solutions that was developed for teething problems with the first turbine, which would have been critical to test before mass producing. Currently, the turbine described below is the only erected by Vertical Wind. Although not having produced any turbines since 2010, Vertical Wind is still active, however at the moment in smaller scale with producing generators for other wind turbine manufacturers. There is also an ongoing effort to find new funding and customers for the development and production of the 200-kW turbines with the possible aim to move on to multi-MW turbines.

The prototype built was erected in 2010 just outside of Falkenberg at the west coast of Sweden and is hereafter referred to as the T1-turbine[4]. It is today owned by Uppsala University and serves as a subject of research in a variety of fields. It has a direct-drive synchronous 36-pole generator with a neodymium-iron-boron permanent-magnet rotor. The generator is designed to have high overload capacity so that all possible operational conditions can be handled. The generator is connected to a frequency converter, situated in a nearby substation, which allows variable speed. As the turbine is not self-starting, the generator is used as a motor (using a separate winding) for a brief period during start-up. Furthermore, the generator is mounted at the bottom of the tower and connected to the rotor by a steel shaft. The shaft is jointed in the middle and supported by two bearings in the top of the tower as well as the bearings of the generator. Since all the moving parts are connected and rotating with the same speed, this configuration can be said to have only one moving part in the entire turbine. The generator has the ability to brake electrically, serving as primary brake system. A hydraulic disc brake placed at the top of the tower works as secondary brake and is used for emergency braking and parking during maintenance.

[4] The specific turbine is called “The T1-turbine” throughout papers I-VII. The name comes from the internal reporting name where T stands for Thorsholm and 1 stands for being the first of planned four turbines. In some publications, the turbine is referred to as “The 200-kW VAWT”.

Figure 1.5: The T1-turbine.

The rotor consist of three 24 m long straight blades that are connected to the shaft by two struts each, both blades and struts are made out of fiberglass. The blades are fixed, but the variable speed of the turbine is used to control the stall effect so that the rated power can be attained between the rated wind speed and the cut-out wind speed. As power control, this can be called electric controlled stall. The turbine is operated from a substation situated 60 m away and the wind speed is measured at a mast 120 m from the turbine. The turbine can also be fully operated by remote desktop.

The T1-turbine has a tower made out of laminated wood covered by fiberglass laminate. In addition to being environmental friendly compared to steel, laminated wood has a lower price-to-strength ratio, making the wooden tower the cheaper option. Additionally, since the blades of the H-rotor cannot pitch in line with the wind, the storm load, i.e. the load on a parked turbine at extreme winds, is considerably higher for an H-rotor than a conventional HAWT. This together with the need to avoid buckling necessitates a certain strength that is difficult to combine with a soft tower (further explained in "2.3 Eigenfrequencies of the semi-guy-wired tower") when using a standard steel tower[5]. Since laminated wood has a higher strength-to-elasticity modulus ratio then steel, a stronger construction can more

[5] This is also due to the lower top mass (compare to a HAWT), prompting a lower elasticity modulus to keep the tower soft (see Figure 2.3 and expression (2.15)).

easily be combined with a soft tower. From the start the tower was freestanding, but after two years it was complemented with three guy wires. The construction may therefore be described as semi-guy-wired. The guy wires were added because small fatigue cracks appeared in some of the glue joints attaching the steel flanges to the glue laminated wood. This is a critical teething problem, as the steel flanges fasten the wood tower to the foundation, which is not intrinsic to the wood tower but rather an effect of bad selection of glue. The problem has been solved and tested by Vertical Wind AB but the solution has not been fitted to the T1-tower for logistic reasons, it would involve the full disassembly of tower and turbine. After adding the guy wires, a new upper limit of the rotational speed was set to 22 rpm. The reason for this is that the added guy wires stiffen the tower so that the first-mode eigenfrequency of the tower is excited at 23 rpm. Also, the frequency of the wire itself has prompted a jump routine around 17 rpm to avoid excitation (further details in section "4.3.1.3 On-site experience").

The T1-turbine is a first prototype and the noise level was not considered during design. If commercially produced, means to minimize noise would probably be taken, for example by smoothing the strut-blade joints.

Other good descriptions of the T1-turbine can be found in [3] which includes a detailed description of the electrical system and [22] which includes a complete summary of the scientific publications.

The T1-turbine can be seen in Figure 1.5 and in Figure 1.6, a schematic illustration of the most important component of the turbine and substation can be seen. The dimensions of the turbine can be seen in Figure 1.7 while Figure 1.8 shows the 3D-cross section and an image of the shaft. Important turbine properties are stated in Table 1.1 while supplementary turbine/tower/wire properties used in calculations throughout this work can be seen in Table 1.2 and Table 1.3.

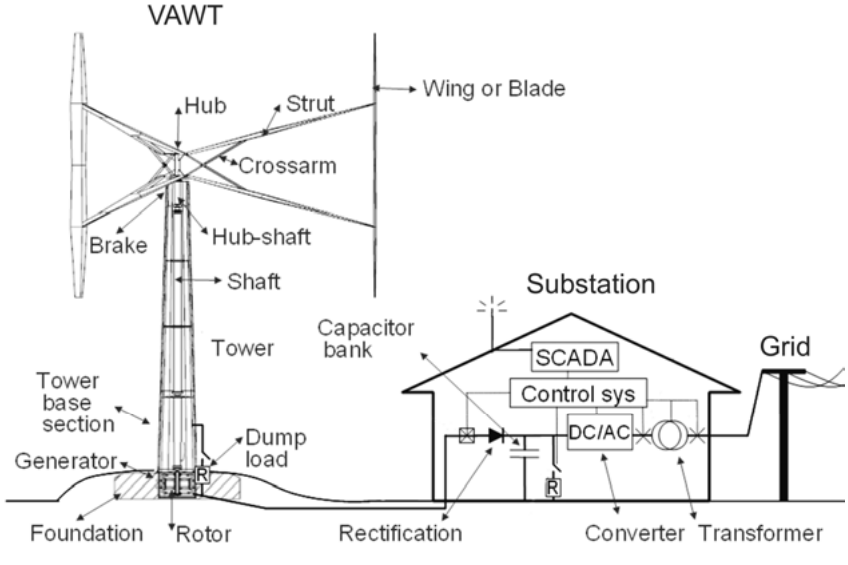

Figure 1.6: A schematic illustration of the T1-turbine and substation [22].

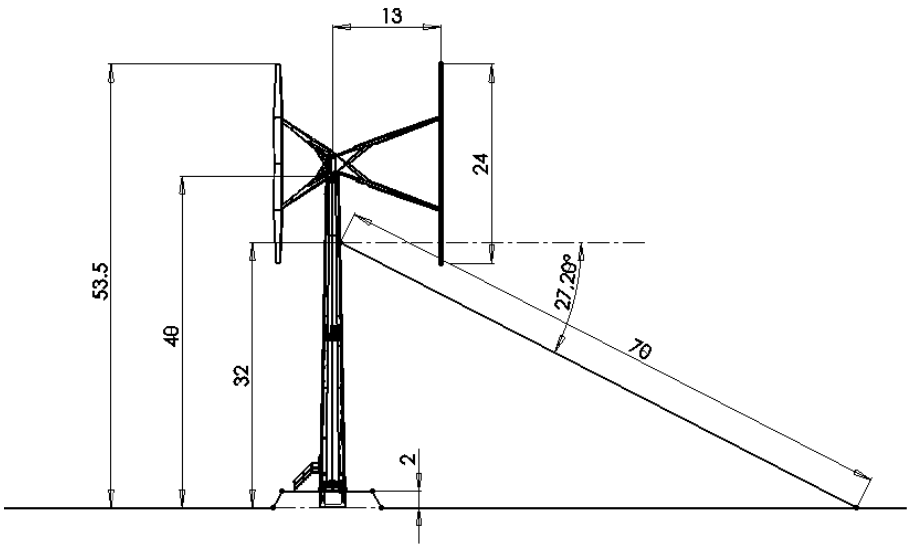

Figure 1.7: Dimensions of the T1-turbine (distances in m).

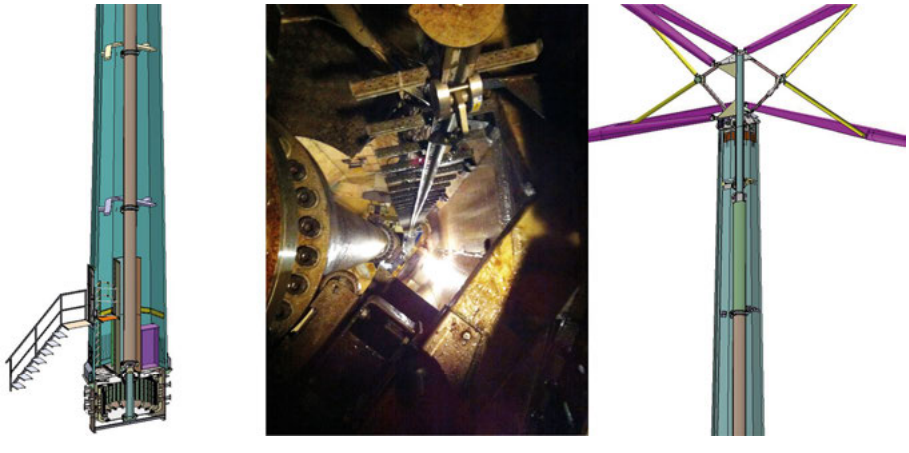

Figure 1.8: Interior and 3D-CAD cross-sections of the T1-turbine.

Table 1.1: *Properties of the T1-turbine.*

Rated power	200 kW
Turbine diameter	26 m
Hub height (incl. foundation)	40 m
Blade length	24 m
Blade chord	0.4-0.9 m
Swept area	624 m^2
Cut-in wind speed	4 m/s
Rated wind speed	12 m/s
Cut-out wind speed	25 m/s
Survival wind speed	60 m/s
Rotational speed	16-33 rpm[6]
Target tip-speed ratio	3.8
Wing/strut material	Fiberglass composite
Tower material	Laminated Wood
Tower shape	Conical dodecagon

Table 1.2: *Supplementary tower/turbine properties used in calculations.*

Tower height	38 m (above ground)
Tower diameter (outer)	2946 mm (base) and 1449 mm (top)
Wall thickness	78 mm
Top mass estimated	10 600 kg
Tower and interior mass estimated	17 000 kg
Density tower material	430 kg/m^3
Elastic modulus E_t	10.5 GPa
C_p used when estimating wind load	0.34

Table 1.3: *Wire properties used in calculations.*

Length of wire L	70 m
Height of guy-wire attachment h	30 m
Axial stiffness $E_w A$	124 MN
Inclination angle between wire and horizon α	27.2°
Linear density μ	5.91 kg/m
Minimum breaking load	1.19 MN

1.1.4 Other contemporary VAWT projects

In recent years there has been a renewed interest in larger VAWTs, not least due to findings within the VAWT research project at the Division for Electricity at Uppsala University which the author of this thesis takes part in. Early-stage large ambition projects worth mentioning are the Danish DeepWind and the French VertiWind which both features floating Darrieus turbines with the aim to produce multi-MW offshore turbines [23, 24].

[6] 33 rpm was the original intended upper limit for rotational speed. After adding guy wires 22 rpm is the new upper limit.

The Polish steel manufacturer Stalprodukt S.A. produces onshore VAWTs, under the brand ANew Institute, ranging up to 200 kW with the aim to design and produce turbines in the >1MW range [25]. For their larger turbines they have a simple and robust 3-bladed concept with a single strut per blade and a steel-lattice towers. It should also be mentioned that they use ground-based generators manufactured by Vertical Wind AB.

There are also several small scale VAWT projects/manufacturers, for example Ropatec [26] from Italy or the Swedish offshore concept SeaTwirl [27] which features a floating tower and, in earlier concepts, a kinetic energy storage using a slow-speed flywheel filled with seawater.

1.2 VAWT research at Uppsala and Halmstad

The VAWT research at the Division of Electricity at Uppsala University has been conducted since 2002 under the lead of division head professor Mats Leijon and professor Hans Bernhoff. In excess of the T1-turbine that is today owned by the division, three smaller VAWTs rating between 1.5 to 10 kW has been built in Marsta just outside of Uppsala. The research at the division has been focusing on various aspects, most prominently generator design and aerodynamics, and has so far resulted in nine doctoral theses [3, 28-35] and several ongoing PhD projects, which includes two licentiate theses [36, 37], which are intended to be extended to doctoral theses in the future. In addition to professors Leijon and Bernhoff, associate professor Sandra Eriksson and postdoctoral researcher Anders Goude are especially prominent within the divisions VAWT research.

Wind power research has been conducted at Halmstad University for some time by professor Jonny Hylander and associate professor Göran Sidén. The collaboration with the Division of Electricity at Uppsala University started in 2012 with Jonny Hylander being co-applicant when the Division of Electricity was granted funding to conduct VAWT research within Uppsala University's participation in the STandUP for ENERGY strategic research framework. As a result of this, the author of this thesis was employed by Halmstad University in 2012 and was as part of the arrangement registered as a PhD student at Uppsala University. The VAWT collaboration was further strengthened in early 2013 when, former employee at the Division of Electricity, Fredric Ottermo was employed as associate professor at Halmstad University, with the intent to continue his work within the VAWT field. The research so far has been focusing on tower dynamics, noise generation and turbulence influence on electric power output for VAWTs.

1.3 About this thesis

This thesis focuses on several different physical aspects of vertical-axis wind turbines, with the 200-kW T1-turbine acting as a reference object for all cases. The work comprises both analytical and experimental work with the scientific goal of

gaining new knowledge as well as verifying existing theories of VAWTs. This has been done partly by capitalizing on the fact that there have been very few H-rotors in the 200 kW range, and using this advantage to study the T1-turbine within three different scientific topics. These topics are: (1) how the wind energy extraction is affected by turbulence, (2) aerodynamical noise and (3) eigenfrequencies of the semi-guy-wired tower.

The seven papers (I-VII) are attached to the printed version of the thesis as appendices. Paper I and II consider how the wind energy extraction is affected by turbulence. Paper III, IV and VII focus on the noise generation. Paper V and VI consider the eigenfrequencies of the semi-guy-wired tower.

The thesis focuses on papers I-VI with the aim to give a context to and merge the results of these papers. The scope of paper VII lies outside that of the two other noise papers (III and IV) and is left outside the merged description although found in whole in the printed version of the thesis. Regarding the thesis outline, the introduction is followed by the following chapters: theory, method, results and discussion, conclusions, summary of papers and author contribution and summary in Swedish. For all chapters, aspects from all three topics are covered.

Some aspects differs between the papers and the thesis. For example, a means to more accurately incorporate the distributed tower mass in the expression for the eigenfrequency of the semi-guy-wired tower, is found in the thesis, as compared to that of paper V. Also, regarding noise, the two proposed models are compared to both measurements rather than only comparing the noise emission measurement to the TBL-TE model and the array measurement to the inflow-turbulence model as in papers III and IV.

Regarding the semi-guy-wired tower, it has been clear from the start that a freestanding tower is preferable, but the installation, forced by the problems with the tower-foundation attachment, has given an opportunity to examine the tower set-up which is the focus here.

2. Theory

2.1 Turbulence and wind energy conversion

Regarding wind turbines, turbulence in the wind is of great importance as it both affects the power output and causes random, fluctuating loads, which stress both the turbine and the tower structure. Turbulence needs to be addressed when designing the turbine, both regarding structural excitation, maximum load and fatigue predictions as well as power control routines [7]. Excessive turbulence has been found to be the most important factor in reducing the life time of a HAWT [38]. The effect of turbulence on wind energy extraction is difficult to generalize since turbulent gusts affects wind alignment, airfoil performance and power control [39]. The influence of turbulence on HAWT power curves has been examined in [40-43] and shows that more turbulence gives higher power for low wind speeds and lower power for wind speeds close to the rated wind speed of the wind turbine. At low wind speeds, these effects are mainly due to the cubic variation of power with wind speed, hereafter called the cubic effect, giving more turbulent winds more power than less turbulent winds with the same mean wind speed. Indeed, the gain from positive deviation will be greater than the loss from negative deviation, which can be seen illustrated in this example: $|(a+b)^3 - a^3| > |(a-b)^3 - a^3|$. As more turbulence will increase the deviation from the mean wind speed value, the mean power will also increase with turbulence.

The impact from turbulence on VAWTs is more complex, not the least because the blades are passing in the turbulent wake of the previous passing blades. Also, because it is omni-directional, it is expected to be less sensitive to horizontal wind fluctuations. In [44], the ability to cope with turbulence for small, urban-sited VAWTs are examined and deemed as good. However, there has been a lack of experimental knowledge on the matter for larger VAWTs.

2.1.1 Power absorption

The available power in the wind for a cross-section area A, can be described by

$$P_{wind} = \frac{1}{2}\rho A v^3, \tag{2.1}$$

where ρ is the density of the air and v the (undisturbed) wind speed. For a vertical-axis wind turbine the cross-section area A is a rectangle, calculated as the turbine diameter multiplied with the blade length. The aerodynamic power coefficient, i.e.

the wind turbine's ability to convert wind energy to mechanical energy, can be defined as

$$C_p = \frac{P_{aero}}{P_{wind}}, \tag{2.2}$$

where P_{aero} is the aerodynamic power output, i.e. the amount of power extracted by the rotor and converted into mechanical power. P_{aero} is related to the electric power output P_{el} according to

$$P_{el} = \eta_d P_{aero}, \tag{2.3}$$

where η_d is the driveline efficiency, i.e. the combined efficiency for generator and mechanical components (see "3.1.2.5 Normalization due to driveline efficiency"). The aerodynamic power coefficient can be described as a function of the tip-speed ratio, λ, which is the ratio between the velocity of the blade tip and the undisturbed wind speed, thus calculated as

$$\lambda = \frac{\omega R}{v}, \tag{2.4}$$

where ω is the angular velocity of the turbine, R is the turbine radius and v is the wind speed. The tip-speed ratio has a large influence on the power coefficient for a wind turbine. To evaluate the performance for all possible tip-speed ratios, a power coefficient curve, often stylized as $C_p(\lambda)$ curve, showing aerodynamic power coefficient as a function of tip-speed ratio can be produced. The control strategy implemented for a variable-speed wind turbine usually applies adapting the rotational speed to the tip-speed ratio for maximum power coefficient, here called $\lambda_{C_{p-max}}$.

2.1.2 Turbulence intensity

In this work, when investigating how the turbulence affects the wind energy conversion, the measure turbulence intensity (TI) is used. The reason for this is both because it is a common measure and as it is available for the case of the T1-turbine. TI stems from the standard deviation of the measured wind speed values, thus it can be obtained using a cup anemometer normally used for measuring wind speed. It is defined as

$$\mathrm{TI} = \frac{\sigma_v}{\bar{v}}, \tag{2.5}$$

where σ_v is the standard deviation of the wind speed for a time period and $\bar{v}$ is the mean wind speed for the same period. The time period used should be longer than the turbulent fluctuations, but shorter than periods associated with long-term wind speed variations such as diurnal effects [7].

With a cup anemometer (which is what is typically used to measure turbulence intensity), only the total horizontal wind speed is measured. A more accurate

quantity for estimating the energy content of the velocity fluctuations within an air volume is turbulence kinetic energy (TKE) which is the mean kinetic energy per unit mass associated with eddies in turbulent flow. TKE stems from the separate standard deviations of the x-, y- and z-directions and, assuming isotropic turbulence as well as using a definition where TI stems from the average velocity fluctuation of the three directions (as commonly used in CFD), it may be related to TI according to [45]

$$\text{TKE} = \frac{1}{2}\left(\sigma_{v_x}^2 + \sigma_{v_y}^2 + \sigma_{v_z}^2\right) = \frac{3}{2}(\text{TI}\ \bar{v})^2. \tag{2.6}$$

Measuring turbulence intensity with a cup anemometer may be problematic, as noted in [46]. For example, mainly the horizontal turbulence is accounted for as the vertical turbulence will have small influence on the horizontal wind speed. It is also generally the case that high TI is accompanied by convective atmospheric conditions and low wind shear [47]. Wind shear affects power production since the mean wind speed varies within the rotor area, affecting the relation between the measured hub-height wind speed and the effective mean wind speed for the rotor area. Using more advanced equipment such as a sonic detection and ranging (SODAR) or light detection and ranging (LIDAR) apparatus, the wind speed can be tracked over the entire height of the rotor and all components of the turbulence can be measured, thus eliminating uncertainties from vertical turbulence and atmospheric conditions. However, cup anemometers are commonly used for measuring TI and while the TI values may be underestimated, the cup anemometer measurements do seem to correctly track changes in turbulence level [46, 47].

2.2 Noise from vertical-axis wind turbines

Sound is a pressure wave that travels through a medium. When discussing sound levels it is important to distinguish between sound power level (noise emission) and sound pressure level (noise immission). The sound power, expressed in watts, represents the rate of sound energy production of a source. The sound power level is proportional to the logarithm of the acoustic power emitted by the source, compared to that of a reference level P_0 of 10^{-12} W, and is given in decibels (dB) by [48]:

$$L_W = 10\log_{10}\left(\frac{P}{P_0}\right). \tag{2.7}$$

Sound power is the most fundamental property of the source but as the intensity diminishes with distance, it is not for the receiver. The effect of one or multiple sources at a specific location can be determined by measuring the sound pressure, which is normally quantified as the root mean square value of the pressure fluctuations that constitutes the sound wave. The sound pressure level is proportional to the logarithm of the square of that pressure compared to that of a

reference value p_0 of 20 μPa (for air). The sound pressure level is given in decibels (dB) by [48]:

$$L_p = 10\log_{10}\left(\frac{p^2}{p_0^2}\right) = 20\log_{10}\left(\frac{p}{p_0}\right). \quad (2.8)$$

The most common way of measuring sound is by measuring all frequencies audible by humans (20-20000 Hz) and presenting it as one single weighted reading [48]. Since the human ear does not have the same perception for all frequencies a filter can be used to account for the relative loudness perceived by the human ear. The most common weight for environment noise assessment and the one generally used in public regulations is the A weight which gives the unit dBA.

The definition of noise is simply unwanted sound. Distinguishing noise from sound is to a large extent subjective, but sound from wind turbines is generally considered as unwanted and therefore it may be referred to as noise. Noise is considered as one of the disadvantages with wind turbines and noise immissions at dwellings and other sensitive areas is generally regulated in national legislation which restrains potential locations when planning for wind power. For example, in Sweden the sound intensity recommendations for noise created by wind turbines is set by the Swedish Environmental Protection Agency (SEPA) to 40 dBA at dwellings which is further lowered to 35 dBA if obvious tones are present in the spectrum. 35 dBA is also the limit for specifically sensitive areas such as nature conservation areas and planned recreational areas [49]. These limits are based on the sound intensity created at a wind speed of 8 m/s, 10 m above ground.

Noise from operating wind turbines can be divided into mechanical and aerodynamic noise with the aerodynamic noise being dominant for modern wind turbines [48]. Mechanical noise originates from the relative motions of mechanical components in the gearbox, the generator, yaw drives, cooling fans, hydraulics and power electronics. Aerodynamic noise is of broadband character and occurs when the air flows around the blade. It originates from various complex flow phenomena and generally increases with tip speed and hence, for a HAWT, the most sound is produced at or close to the tip of the blade. Most of the audible aerodynamic noise is created when the blade travels downwards towards the receiver, a result of the directivity of aerodynamic noise emitted from a moving airfoil [48]. The characteristically swishing sound of a wind turbine is due to amplitude modulation and has been proven to be the sound feature from wind turbines that is the most annoying [48]. This mid frequency phenomena (400-1000 Hz) is created by the directivity of the trailing-edge-noise.

Extensive research has been presented regarding noise from wind turbines. For example, interesting work can be found in [50] where the effects of natural sounds on sound modelling, masking and propagation has been studied and in [51] where the human response to wind turbine noise has been investigated. However most research has been aimed at the more common HAWT concept and little attention has been given to the alternative VAWT concept which has shown potential for lower noise levels.

VAWTs usually have lower tip-speed ratio than HAWTs. The entire length of a VAWT blade travels at tip speed, which for a HAWT is only true for the actual blade tip. Since it has been shown that most of the aerodynamic noise from a HAWT is generated close to the tip [52], the blade velocity where noise is produced is lower for a VAWT then for a HAWT, an argument for lower levels of aerodynamic noise. However, the reality is more complex, mainly due to the unsteadiness of the flow. An additional difference is that VAWTs usually have support arms carrying the blades, a feature not needed for HAWTs. In addition, tonal components, mainly harmonics of the blade-passing frequency, is generally expected to be present in the VAWT noise spectrum due to the unsteady blade loading [53]. This should however mainly be an issue for small-scale VAWTs as the blade-passing frequency and major part of its harmonics fall outside the audible frequency range for larger VAWTs. Furthermore the drive train of a VAWT can be located at ground level which limits mechanical noise propagation.

Work that has been performed regarding noise from VAWTs include [54] and [55] where numerical methods are used to simulate aerodynamic noise from VAWTs and which for both studies indicates lower noise levels compared to HAWTs. In [53], microphone array (a.k.a. noise camera) measurements were performed on a down-scaled VAWT in a wind tunnel, indicating that at low tip-speed ratio, the dominant noise sources are found in the upstream half of the rotation (interpreted as due to dynamic stall), while at higher tip-speed ratio the dominant sources where found in the downstream half.

2.2.1 Aerodynamic noise prediction models

With the aim to investigate which noise source that is most important for the T1-turbine, existing models of the two most interesting noise mechanisms are adapted for the VAWT case and used for comparison with measurements (in “4.2.3 Comparison with noise prediction models”).

Aerodynamic noise sources can be divided depending on causation, most notably airfoil self-noise and inflow-turbulence noise. Airfoil self-noise is caused by the interaction between the turbulence created by the blade and the airfoil itself [56]. The airfoil self-noise sub-group turbulent-boundary-layer trailing-edge noise (TBL-TE) noise is created when the turbulent boundary layer, that develops along the blade surface and convects downstream, passes the trailing-edge. The sudden change when the blade surface disappears causes sound to be scattered as broadband noise. In [52], microphone array measurements showed that for a modern HAWT, TBL-TE noise is the dominant noise source. Other airfoil self-noise sub-groups include tip noise, blunt trailing-edge noise, separation-stall noise and laminar-boundary-layer vortex-shedding noise. For more information about these and other sub-groups, well explained descriptions can be found in [48].

The inflow-turbulence noise is created when upstream turbulence interacts with the leading edge of the blade [48]. The sound originates when the turbulent eddies is scattered at the leading edge, creating noise of broadband character. This noise source is dependent on the amount of incoming turbulence, hence both the

atmospheric conditions and the eventual presence of turbulence creating structures in the vicinity, such as other wind turbines, will be of importance. It is to some grade an open issue to what extent inflow-turbulence noise contributes to the overall noise level of a wind turbine [48], although it has been shown that it is not the dominant effect for a large-scale HAWT [52]. However, the contribution of inflow-turbulence noise can be assumed to be greater for VAWTs than HAWTs as the blades are passing in the turbulent wake of the previous passing blades.

2.2.1.1 TBL-TE noise model

Guided by the fact that HAWT noise is well modeled by the TBL-TE noise contribution, we try to estimate the noise level by using the TBL-TE part of the empirical model for airfoil self-noise in [56]. For small VAWTs (low Reynold numbers), laminar-boundary-layer trailing-edge noise has been observed to be important [53], but for the larger-sized turbine considered here the Reynolds number is of the order of $1 \cdot 10^6$, so the TBL-TE is expected to be dominant over the laminar-boundary-layer part. A complication is that the model in [56] assumes static angles of attack, whereas in this case the angle of attack is constantly changing. However, static angle-of-attack lift and drag data has been successfully used in prediction models of VAWT performance [10], so it is reasonable to evaluate a static approach here as well. Further information about the reasoning behind omitting the dynamic stall effect spawned from the varying angle of attack as well as the model itself and its application is described in Paper III[7].

2.2.1.2 Inflow-turbulence noise model

An important difference between VAWTs and HAWTs with respect to noise generation is that the blades of a VAWT, at the downstream half of the rotation, pass the wake of the blades at the upstream half. The turbulence levels at the downstream half of a VAWT is then expected to be much larger than the turbulence of the flow ahead of the turbine, due to the upstream blade disturbing the flow. Inflow-turbulence has been proposed to be a significant source of noise even for HAWTs, depending on the turbulence properties of the incoming flow [48]. The flow of a small 2-bladed VAWT was mapped experimentally in [57], and, as can be observed in for example Figure 2.1 which shows results from that work, a significant amount of turbulence is generated by the blades and struts. The velocity fluctuations appears to be dominated by the tip vortices, but a significant amount of turbulence is also seen to be generated by the struts and the tower, apparently a lot more than the contribution from the trailing-edge vorticity. The tip-vortex trajectories expand with the widening of the flow and do not seem to cross the paths of the blades behind, as they move from the most downstream position towards the most upwind position. However, the turbulence generated by the tower and the struts is indeed observed to collide with the downstream blade path. This means that inflow-turbulence noise

[7] A more detailed description of the TBL-TE model (found in Paper III) was left out of the thesis as it in the end was shown to be of little importance for the VAWT case.

might be a potential noise source for VAWTs, irrespective of the atmospheric properties.

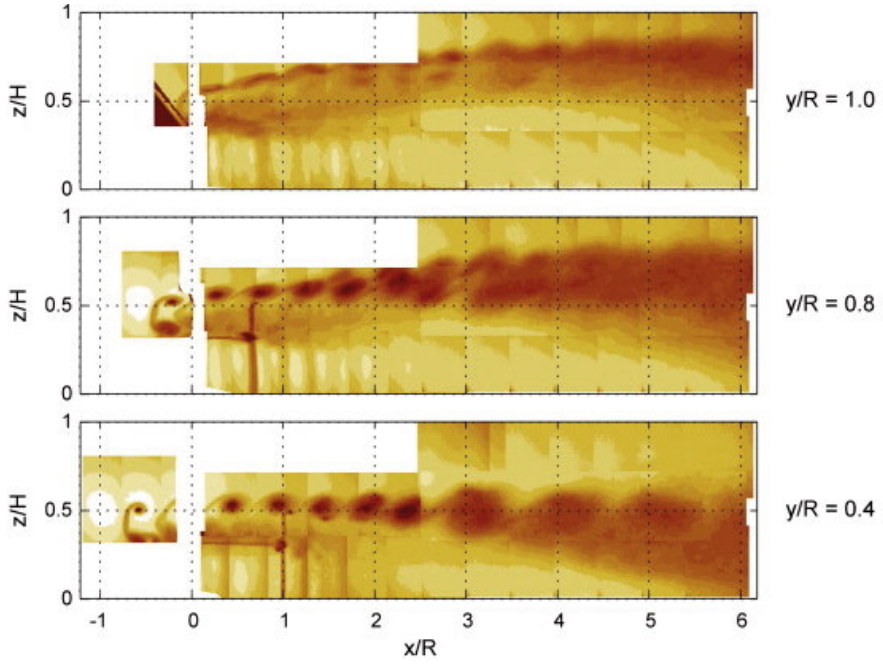

Figure 2.1: Absolute velocity fluctuations for three parallel vertical planes on the "blade moves opposite wind direction" half. Darker color tone means larger velocity fluctuations. The location of the vertical plane is given by y where y=0 is the center plane and y=R is tangent to the blade trajectory. x denotes the distance in the wind direction where x=0 is the tower location. The blade stretches between z=-0.5H to z=0.5H, i.e. the image only shows the upper half. The figure is a part of Figure 17 in [57] and republished with permission from the authors of that work.

A semi-empirical model for inflow-turbulence noise has been used in the context of HAWTs [58-61], for inflow-turbulence produced by the atmospheric boundary layer. In [61] the model was compared to an extensive set of experimental data, accompanied with an accurate determination of the inflow-turbulence characteristics. The model was found to predict the measure noise level reasonably well in the mid-frequency range (which will be the range of interest here). According to this model, the sound-pressure level, in 1/3-octave bands, is [58]

$$L_p = 10\log_{10}\left(\frac{\rho_0^2 c_0^2 l_t L_s}{2r_e^2} M^3 v^2 \mathrm{TI}^2 \frac{(K/K_e)^3}{(1+(K/K_e)^2)^{7/3}} \cdot \frac{\mathrm{LFC}}{1+\mathrm{LFC}} \overline{D}_L\right) + 78.4, \qquad (2.9)$$

with SI units for all parameters, where ρ_0 is the density of air, c_0 is the speed of sound, l_t is a turbulence length scale, L_s is the blade span (segment), r_e is, as earlier mentioned, the retarded distance to the observer, M is the Mach number of the local velocity over the airfoil and v is the undisturbed wind speed. TI is the turbulence

intensity as given by equation (2.5). K is the local wavenumber, K_e is the wavenumber of the energy-containing wavelength scale of the turbulence, LFC is a low-frequency correction[8] and $\bar{D}_L$ is the directivity factor (as the one of a translating dipole) which can be written as

$$\bar{\mathrm{D}}_L \approx \frac{\sin^2\theta \sin^2\varphi}{(1+M\cos\theta)^4}. \tag{2.10}$$

The angles θ and φ can be seen in Figure 2.2 for a source at the leading edge of the airfoil. The retarded position of the observer is calculated using the free-stream wind speed, see [53], and the angles θ and φ are calculated with respect to the retarded position. The local Mach number M (as well as the local wind speed when used) is here calculated using a simple flow model where the flow is unperturbed by the turbine. The Doppler shift is also neglected as the shift in intensity and frequency will be within 0.5 dB and 5% respectively for the velocities encountered.

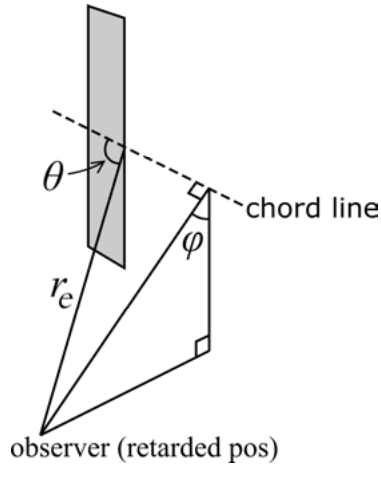

Figure 2.2: Definition of the angles θ and φ and the retarded distance r_e for a source at the leading edge of a vertical blade. The angles are calculated with respect to the retarded position of the observer.

The model is sensitive to the turbulence length scale l_t. For the case of atmospheric turbulence in the context of HAWTs, the integral length scale of the turbulence has been commonly used [58]. Here we assume that the majority of the inflow-turbulence is due to the turbine itself, and the corresponding length scale is not obvious, but the chord length (~1 m) or blade thickness (~0.2 m) appears as a reasonable guess, or possibly the larger structures of the turbine (~10 m). Moreover, the model assumes a homogeneous spectrum of frequencies, whereas it is reasonable

[8] The wavenumbers K and K_e as well as the low-frequency correction LFC is explained in more detail in Paper IV, section "2.1. Inflow-turbulence noise modeling".

to expect that certain frequencies might dominate for the turbulence generated by the turbine.

2.2.1.3 Application of the inflow-turbulence noise model

To use the model in equation (2.9) for noise prediction of the T1-turbine, assumptions are needed, especially regarding the turbulence intensity.

The extra turbulence produced by the struts and joints must be accompanied by a loss in converted power. If the struts were (hypothetically) removed, we expect the power coefficient to be of the order of a Darrieus turbines (a.k.a. Full-Darrieus turbine, the egg-beater design without struts), which have been reported to achieve $C_p = 0.4$ or slightly better [4]. Indeed, ignoring drag due to the presence of the struts, the H-rotor is expected to allow for better aerodynamic performance than the Darrieus [10, 62]. For the Darrieus turbine, part of the blade will operate in the stall region of the cross-section area, decreasing the contribution from these parts. Since the power coefficient of the T1 turbine is (as shown in "4.1.1 Turbulence influence on power curves and power coefficient") about $C_p = 0.33$, we may assume a power-coefficient loss of $\Delta C_p = 0.07$ due to the presence of the struts. The corresponding power loss at hub-height wind speed $v = 6$ m/s will be

$$\Delta P = \frac{1}{2}\Delta C_p \rho_0 A v^3 \sim 5.7\ kW, \tag{2.11}$$

using air density $\rho_0 = 1.2$ kg/m^3 and rotor cross-section area $A = 26 \cdot 24$ m^2. The extra kinetic energy contained within a volume V due to the turbulence is $\Delta E = \rho_0 V \cdot \mathrm{TKE}$ (for TKE, see equation (2.6)). Assuming that this power loss is contained in an extra amount of air turbulence that is convected with the flow, the corresponding turbulence intensity may be calculated from equation (2.6) by rearranging as

$$\mathrm{TI} = \frac{1}{\bar{v}}\sqrt{\frac{2}{3}}\mathrm{TKE} = \frac{1}{\bar{v}}\sqrt{\frac{2}{3}}\Delta P/(\rho_0 \dot{V}) \sim 0.40. \tag{2.12}$$

Here, the volume flow rate is $\dot{V} = A_t v_{loc}$, where v_{loc} is then local velocity and A_t is the cross-section area of the turbulent volume convecting downstream. A_t is estimated from Figure 4.12 to be $2 \cdot 10$ m^2 at the position where noise is emitted, which is where we are interested in the turbulence intensity (shortly after the blade-strut joint, where the turbulence is expected to be created, the area is smaller and the turbulence intensity larger). The local velocity is estimated as $V \approx v + v_{blade} = 28$ m/s, since most of the noise is created when the blade moves towards the wind. Furthermore, for equation (2.12) to hold, it is assumed that each blade contribute to the power loss accordingly during one third of the turn, effectively. Note that the turbulence intensity estimated in (2.12) is much larger than the ambient turbulence intensities given in Table 3.1, which appears reasonable given the measurements in [57].

Using this value of the turbulence intensity (which we assume to be valid for a range of wind speeds around 6 m/s), it is possible to use equation (2.9) to estimate the corresponding emitted sound spectrum in the different directions. The turbulence length scale is taken to be l_t = 0.2 m, and the blade span where sound is emitted is estimated from the pictures to be L_s = 10 m. Guided by the source maps (see "4.2.2 Microphone array measurements"), the sound is modeled to originate from two regions, one in the upper region and one in the lower region of the blade. The sound is further modeled to be emitted during a distance of 5 m per blade around the azimuth angle β = 88° (again from the results, see "4.2.2 Microphone array measurements").

2.2.2 Measuring noise emission from a wind turbine

When recording noise from a wind turbine, the sound recorded $L_{p,rec}$ (in dBA) consists of the sound pressure level due to the wind turbine noise $L_{p,wt}$ as well as the background sound $L_{p,bg}$ which are related by [48]:

$$L_{p,rec} = 10\log_{10}\left(10^{\frac{L_{p,wt}}{10}} + 10^{\frac{L_{p,bg}}{10}}\right). \tag{2.13}$$

Recording with the wind turbine sequentially turned on and off, equation (2.13) can be used to separate the wind turbine sound pressure level from the total sound level, if the wind and background sound conditions are unchanged. In reality, the conditions are never unchanged. But by keeping track on the wind speed and using long enough recordings, the effect of wind speed can be taken into account and the effect of background sound conditions will be evened out. The emitted sound pressure levels of the wind turbine can then, by taking the spherical sound distribution and the coherent addition of sound reflected from the ground b (typically 6 dB), be used to calculate the emitted sound power level (a.k.a. and hereafter referred to as noise emission) $L_{W,wt}$ (in dBA) of the wind turbine by:

$$L_{W,wt} = L_{p,wt} - b + 10\log_{10}\left(\frac{4\pi R_{obs}^2}{S_0}\right), \tag{2.14}$$

where S_0 is a reference area of 1 m^2 and $R_{obs} = \sqrt{R_h^2 + H^2}$ is the distance between the rotor axis at hub height and the place of recording, where H is the hub height of the turbine and R_h the horizontal distance between the tower and the place of recording. The standardized measurement procedure for deciding the noise emission is described in the International Electrotechnical Commission (IEC) standard "Wind turbines – Part 11: Acoustic noise measurement techniques" IEC61400-11 [63] and a similar but not identical approach has been used for this work (see "3.2.1.4 Measurement limitations" for deviations from standard).

2.2.3 Locating noise sources with a microphone array

Location of the aerodynamic noise sources for a wind turbine, i.e. quantifying where in a scanning grid (2D or 3D) the noise originates, is of great interest as is allows for deeper understanding of the underlying mechanisms of the noise[9].

The location can be done using a microphone array (sometimes called noise camera or acoustic camera) consisting of a number of microphones situated in a plane with its normal directed toward the noise source of interest. Since there is a difference in distance from the source to the different microphones, a sound wave emitted at a certain position in the scanning grid will arrive at each microphone at different times, which is observed as a phase shift between the measured signals. Furthermore, since the pressure amplitude decreases with distance, it will differ between the microphones. The noise can then be localized by using so called delay-and-sum technique (beamforming), which means delaying each microphone signal relatively and adding them, thus the signal coming from a specific scanning-grid position will be amplified while other signals will be suppressed. By plotting the amplitude for different positions, an acoustic map can be obtained, i.e. an image color grading the source plane by noise generation [48]. The delay-and-sum method has drawbacks, for example the produced acoustic map has artifacts which have to be removed by using an algorithm such as the Deconvolution Approach for the Mapping of Acoustic Sources (DAMAS) [64]. Additionally, diagonal deletion of the cross-spectral matrix is often used to improve the source-maps by removing the wind-induced contribution to the diagonal of the matrix [65].

2.3 Eigenfrequencies of the semi-guy-wired tower

An eigenfrequency is a frequency at which a construction tends to oscillate in the absence of driving or damping forces [66]. If the eigenfrequency coincide with a forced frequency, a so called dynamic load, the amplitude of vibration escalates and resonance occurs. A construction has several different eigenfrequencies, different modes, where for each frequency the construction is moving in a different way. Eigenfrequencies of a structure depend on material, shape, dimensions, mass as well as motion constraints such as guy wires.

Instability due to eigenfrequencies is of concern regarding wind turbines as well as most other tall structures. Different components of a wind turbine can have their own eigenfrequency and besides the tower which is the main subject of this work, the T1-turbine's mode shapes due to the elasticity of the struts has been examined in [67] and for the driveshaft in [68]. In [67], it was found that by careful dimensioning it is possible to obtain a large resonance-free operational rotational-speed range regarding the struts. The aerodynamic damping of the eigenmodes of interest was also found to be good. In [68] it was found that by using a directly-driven generator, the shaft can be made considerably smaller. Furthermore, the Sandia National

[9] For more information of the stationary 2D scanning grid used in this work and why it is deemed sufficient, see Paper IV, section "2.3 Beamforming".

Laboratories VAWT research of the 1970-80s includes work on guy-wired VAWTs, for example vibration and damping issues of the guy wires [69, 70]. Sandia studies a Darrieus turbine supported entirely by guy wires attached to the top, whereas the VAWT studied in this work is only partly guy wire supported.

For the tower of a typical wind turbine, it is mainly the first-mode eigenfrequency (i.e. the simplest oscillation and thus the lowest eigenfrequency value) that is of interest since it may coincide with a dynamic load of the turbine. The dynamic loads of significance are imbalances in the shaft or rotor as well as aerodynamic loads of the passing blades. The frequencies of these loads are 1P and 3P respectively, where P is the rotational speed of the turbine. The rotational speeds where the eigenfrequencies are excited by the dynamic loads are $n = 60 \cdot f$ (rpm) and $n = 20 \cdot f$ (rpm) for 1P and 3P (as there are three blades) respectively where f is the eigenfrequency.

When designing a wind turbine tower, different strategies can be used to avoid resonances due to the dynamic loads. The tower can be made stiff which means that the eigenfrequency is placed above the 3P load for the entire operational range. The tower can also be made soft which means that the eigenfrequency is placed between the 1P and 3P loads or even soft-soft with the eigenfrequency placed below the 1P load. In Figure 2.3, these strategies for an operational range typical for a modern 3MW HAWT can be seen. For the soft and soft-soft towers, the eigenfrequencies are briefly excited when ramping up rotational speed during start-up, but are not located within the operational range. For modern large scale wind turbines, soft towers are the most common, this because it is usually a good trade-off between stability and economy.

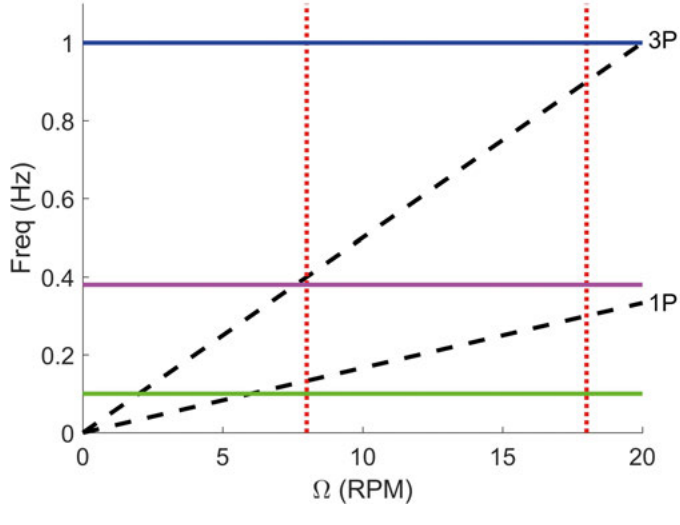

Figure 2.3: A Campbell diagram showing a stiff tower (blue), soft tower (magenta) and soft-soft tower (green). Operational range marked with red dashed lines.

2.3.1 First-mode eigenfrequency of a semi-guy-wired tower

In this chapter, an expression for the eigenfrequency of the one-of-a-kind tower set-up of the T1-turbine is derived (the validity of the expression is later investigated in "4.3.1 Eigenfrequency of the semi-guy-wired tower").

For a typical freestanding tower, the first-mode eigenfrequency can be approximated by using a fairly straightforward expression (2.15) for a vertical massless uniform beam of length H, with the lower end attached to the ground and a point mass m attached to the top [71].

$$f = \frac{1}{2\pi}\sqrt{\frac{3E_t I}{mH^3}}. \tag{2.15}$$

Here, E_t is the elasticity modulus of the tower material, and I the second moment of area of the beam. However, the T1-turbine is a near unique case since it was freestanding from the start but since has been complemented with guy wires, thus making it both firmly bolted to the ground and constrained at a certain height by the guy wires – hence there is no suitable ready-made expression available to use.

If the guy wires are attached to the tower at height h, a force has to be included that counteracts the tower movement, making the frequency calculation more complex. The net force from the guy wires can be divided into z- and x-components, F_z and F_x, where the vertically acting F_x can be neglected due to its minimal effect on the tower movement for small deviations. The effect from the torque connected to the mass distribution of the rotor is also deemed small and neglected (this effect is investigated in "4.3.1.1 Simulation of tower eigenfrequency"). In addition to the top point mass, the distributed tower mass will also have an effect which is disregarded at first but in "2.3.3.3 Incorporating tower mass" a means of incorporating the effect is retrieved.

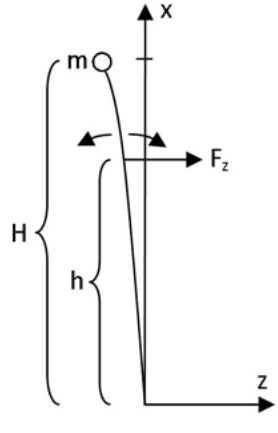

Figure 2.4: The tower modeled as a massless uniform beam with a mass m on top. H is the height of the tower, h is the height of guy-wire attachment point and z is the horizontal deviation.

The z-deviation of the tower may be written on the form $z = W(x,t) = w(x)\sin(\omega t)$. Using Euler-Bernoulli beam theory with constant mass distribution μ, we have [72]

$$E_t I \frac{\partial^4 W}{\partial x^4} = -\mu \frac{\partial^2 W}{\partial t^2} + Q, \tag{2.16}$$

where $Q(x,t)$ is a distributed force along the beam. Assuming that the distributed force also has a $\sin(\omega t)$ time dependence, so that $Q(x,t)=q(x)\sin(\omega t)$, this simplifies to

$$E_t I w^{(4)}(x) = \mu\omega^2 w(x) + q(x). \tag{2.17}$$

This particular time dependence for the distributed force appears for external spring forces on the beam. Point forces (with the same time dependence) and point masses along the beam may be incorporated into equation (2.17) by using Dirac delta functions. Equivalently, such forces and masses may be introduced as boundary conditions if $w(x)$ is split into pieces, splitting at the positions of the point forces or point masses. Therefore we split $w(x)$ according to

$$w(x) = \begin{cases} w_1(x), & 0 \le x \le h, \\ w_2(x), & h \le x \le H, \end{cases} \tag{2.18}$$

since we indeed have a point force at $x=h$. The point force (at $x=h$) and point mass (at $x=H$) now appear as boundary conditions for the third derivate (which relates to the shear force in the beam),

$$\begin{cases} E_t I(w_1'''(h) - w_2'''(h)) = -F_z, \\ E_t I w_2'''(H) = -m\omega^2 w_2(H), \end{cases} \tag{2.19}$$

where F_z is the z-component of the net force from the guy wires when the tower has the form $w(x)$, and m is the point mass at the top. F_z is a spring force and depends on the deviation at the height h,

$$F_z = -\tilde{k} w_1(h), \tag{2.20}$$

where $\tilde{k}$ is the effective spring constant for F_z with respect to the horizontal deviation of the tower at $x = h$ (note that since F_z is a spring force, proportional to the tower deviation, the previously assumed time dependence of the forces applies). The relation between $\tilde{k}$ and the spring constant k of the individual guy wire is derived in section "2.3.3.1 Effective spring constant of guy wire" nedan. The remaining boundary conditions for the differential equation (2.17) are

$$\begin{gathered} w_1(0) = w_1'(0) = 0, \quad w_2''(H) = 0\,, \\ w_1(h) = w_2(h), \quad w_1'(h) = w_2'(h), \quad w_1''(h) = w_2''(h). \end{gathered} \tag{2.21}$$

The conditions at $x = 0$ is due to the beam being fixed to ground, and $w_2''(H) = 0$ is a consequence of the absence of moment of inertia at the top. The conditions at $x = h$ follows from continuity of the beam position, beam slope and moment at that point.

There are no distributed forces in this case ($q(x) = 0$). In addition, by assuming a massless beam ($\mu = 0$) it is possible to obtain an analytic expression for the frequency. For this case we obtain polynomial solutions,

$$\begin{aligned} w_1(x) &= A_1x^3 + A_2x^2 + A_3x + A_4, \\ w_2(x) &= B_2x^3 + B_2x^2 + B_3x + B_4. \end{aligned} \tag{2.22}$$

Using the eight boundary conditions, we get a homogenous linear system of equations for these eight integration constants. Requiring a nontrivial solution, the determinant of the system of equation has to be zero, which leads to

$$\left(1 - \frac{C_1H^3}{3}\right)\left(1 + \frac{C_2h^3}{3}\right) = -\frac{C_1C_2}{4}\left(Hh^2 - \frac{h^3}{3}\right)^2, \tag{2.23}$$

where $C_1 = m\omega^2/(E_tI)$ and $C_2 = \tilde{k}/(E_tI)$. As $f = \omega/(2\pi)$, this implies a frequency

$$f = \frac{1}{2\pi}\sqrt{\frac{E_tI}{m} \cdot \frac{1 + \frac{\tilde{k}h^3}{3E_tI}}{\frac{H^3}{3} + \frac{\tilde{k}}{E_tI}\left(\frac{H^3h^3}{9} - \frac{1}{4}\left(Hh^2 - \frac{h^3}{3}\right)^2\right)}}. \tag{2.24}$$

We note that the frequency without guy wires is retrieved for $\tilde{k} = 0$. In the case of a massless tower, there will only be one mode of oscillation. Higher order modes are possible only if there is distributed inertia (mass) along the tower.

It would be relatively straightforward to extend the model to allow for different second moment of areas above and below $x = h$. This would to some extent mimic the tapering of the beam. Such an extension has however not been further explored here. See section "2.3.3.2 Second moment of area" for how the second moment of area of the T1-turbine tower was chosen when used in the model.

2.3.2 Effect of wind force upon guy wire first-mode eigenfrequency

In the case of a guy wired tower, the eigenfrequencies of the wires also becomes of significance. Resonance of the guy wires will produce amplified motions that in worst case can destroy the entire tower [73]. Just as for the tower, it is mainly the first mode of eigenfrequency that is of interest since it may be excited by the tower

or blade-passing frequencies. The eigenfrequency of the wire can be described as that of a vibrating string

$$f = \frac{1}{2L}\sqrt{\frac{T}{\mu}}, \tag{2.25}$$

where T is the tension, μ is the linear density and L is the length of the string. For an unloaded tower, the tension T is simply the pre-tension which is applied to the wire. However, a structure which is subject to large loads, like a wind turbine, T will alter and the eigenfrequency will vary with the load, which in this case is linked to the wind speed.

We can divide the tension T in pre-tension T_p and tension from the wind force ΔT, where ΔT can be obtained by $\Delta T = k\Delta W$, where k is the spring constant and ΔW is the extension of the wire.

For a supporting guy wire, ΔW can be described by $\Delta W = \Delta Z \cos\alpha$, where ΔZ is the horizontal deviation at the height of guy-wire attachment and α is the angle between the guy wire and the horizon.

$$f = \frac{1}{2L}\sqrt{\frac{T_p + k\Delta Z\cos\alpha}{\mu}}. \tag{2.26}$$

Using the same method as in "2.3.1 First-mode eigenfrequency of a semi-guy-wired tower" but modifying (2.19) for static displacement instead of motion we get

$$\begin{cases} E_t I(w_1'''(h) - w_2'''(h)) = -F_z, \\ E_t I w_2'''(H) = -F_T, \end{cases} \tag{2.27}$$

where F_T is the thrust force, i.e. the wind load acting on the rotor, which in a simplified way can be obtained by multiplying the maximum total wind force that possibly could act on the swept area with the thrust coefficient C_T. The maximum wind force can be obtained by dividing the available power in the wind (from equation (2.1)) with the wind speed, giving

$$F_T = \frac{1}{2} C_T \rho A v^2. \tag{2.28}$$

C_T is always larger than C_p but for a turbine with low solidity (low axial induction factor in the Betz turbine calculation), they can as an approximation be estimated as equal [7].

Using a similar approach as for the dynamic case in "2.3.1 First-mode eigenfrequency of a semi-guy-wired tower" and using the boundary conditions in (2.21), leads to the following expression[10]

[10] For a detailed derivation, see paper VI.

$$w_1(h) = \Delta Z = \frac{F_{wd}}{2E_t I} \cdot \frac{Hh^2 - \frac{h^3}{3}}{1 + \frac{\tilde{k}h^3}{3E_t I}}. \quad (2.29)$$

By combining (2.29) with (2.26), we obtain the eigenfrequency of a windward wire in line with the wind direction for different wind loads. Using a negative ΔZ in (2.26) will give the eigenfrequency for a leeward wire. Since ΔZ will be largest for a wire in line with the wind, the eigenfrequencies of all wires independent of angle towards wind direction will be covered within those of the windward and leeward wires, creating a frequency range where resonance is likely to occur.

2.3.3 Effective spring constant, second moment of area and tower mass

2.3.3.1 Effective spring constant of guy wires

The spring constant of a single guy wire is given by $k = E_w A/L$, where $E_w A$ is the axial stiffness of the wire, which in turn is a product of the elasticity modulus of the wire material and the cross-section area of the wire. L is the length of the wire. The effective spring constant $\tilde{k}$ introduced in "2.3.1 First-mode eigenfrequency of a semi-guy-wired tower", on the other hand, is related to the horizontal component F_z of the net force from all the guy wires and the displacement ΔZ of the tower, so that $\tilde{k} = F_z/\Delta Z$.

Initially considering the force F_w from one guy wire (see Figure 2.5), the horizontal component of this force is $F_{1h} = F_w \cos\alpha$, where α is the wire-inclination angle. A displacement ΔZ of the tower, in the direction of the guy wire, changes the wire length by the amount $\Delta W = \Delta Z \cos\alpha$. Since $\Delta F_w = k\Delta W$, we get

$$\Delta F_{1h} = k\Delta \quad (2.30)$$

Now, including the second and third guy wires, we note that these wires, as seen from above, form an angle 60° to the displacement direction (see Figure 2.6). As a consequence, the length of these wires changes by $\Delta W_{2h} = \Delta W \cos 60° = \Delta Z \frac{\cos\alpha}{2}$. This means that the horizontal force component F_{2h} and F_{3h} of these wires changes according to

$$\Delta F_{2h} = \Delta F_{3h} = k\Delta Z \frac{\cos^2\alpha}{2}. \quad (2.31)$$

The net horizontal force F_z now becomes

$$F_z = \Delta F_{1h} + \Delta F_{2h} \cos 60° + \Delta F_{3h} \cos 60° = 1.5k\Delta Z \cos^2\alpha, \quad (2.32)$$

from which we deduce that

$$\tilde{k} = 1.5k \cos^2\alpha. \quad (2.33)$$

If the wind direction is not in line with one of the guy wires, the results is unchanged, which can be shown by incorporating an arbitrary deviation angle in the calculation above.

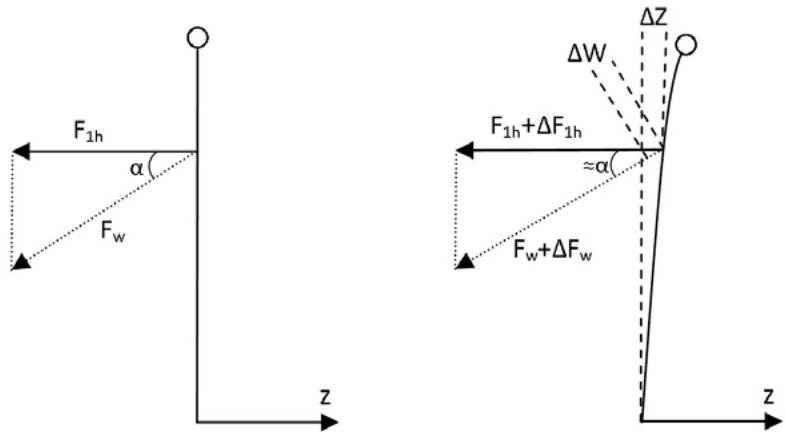

Figure 2.5: Spring forces seen from side. Left: Forces acting for centered tower. Right: Forces acting after displacement.

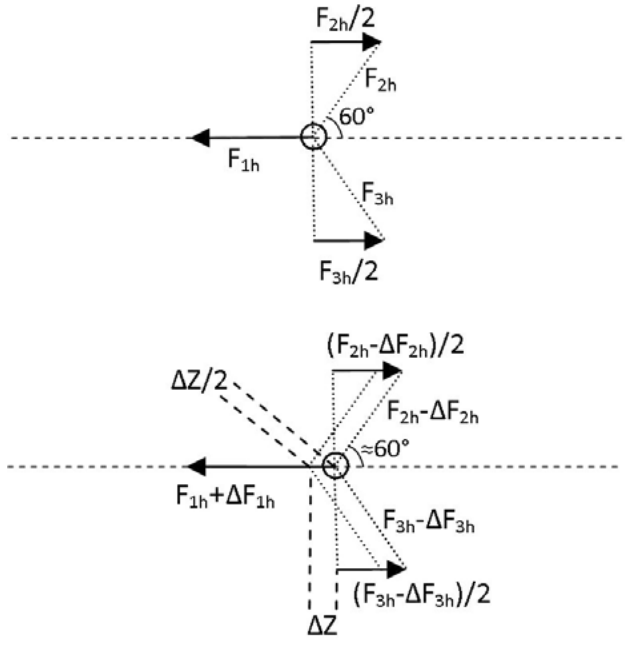

Figure 2.6: Spring forces seen from above. Upper: Forces acting when in rest. Lower: Forces acting after displacement.

2.3.3.2 Second moment of area

The second moment of area for a circular pipe can be calculated by

$$I=\frac{\pi}{64}(d_{out}^4 - d_{in}^4), \tag{2.34}$$

where d_{out} is the outer diameter and d_{in} is the inner diameter of the pipe cross-section [74]. For a conical tower the simplest approach is to use the mean outer and inner diameter of the conical tower to represent the pipe. A more correct approach would be to take the average of I using the diameter at the top and the bottom, this since d_{out} and d_{in} is raised with an exponent of four. However, when using guy wires, the impact of the second moment of area is assumed to be largest where the wires are attached since the lower part of the tower will be prevented from moving and thus this height will be the reference position for oscillation. Therefore, for the case with guy wires, I is calculated using d_{out} and d_{in} for $x = h$.

In reality, the cross-section shape of the T1-tower is not round but dodecagonal. However, using a round cross-section for simplicity is estimated to have a small impact on the results.

Table 2.1: *The second moment of area of the T1-turbine's tower by using a) the average inner and outer diameter, b) the average of the second moment of area for the top and bottom and c) the inner and outer diameter for the height h.*

	d_{out} (m)	d_{in} (m)	I (m^4)
a	2.198	2.042	0.292
b	2.946 and 1.449	2.790 and 1.293	0.401
c	1.764	1.608	0.147

2.3.3.3 Incorporating tower mass

For an unsupported tower, the distributed tower mass can be incorporated into expression (2.15) by replacing m with the effective top mass m_{eff} with about 1% uncertainty [71]:

$$m_{eff} = m + 0.24m_{tower}. \tag{2.35}$$

Since the guy wires prevent the lower parts of the tower from moving, this expression will not be an as exact solution for the semi-guy-wired case.

A tower mass can be introduced by putting $\mu = m_{tower}/H$ in equation (2.17). The solution is then more complicated and a no-analytical expression for the first-mode frequency may be obtained. We get

$$\begin{aligned} w_1(x) &= A_1\sinh(\beta x) + A_2\cosh(\beta x) + A_3\sin(\beta x) + A_4\cos(\beta x), \\ w_2(x) &= B_1\sinh(\beta x) + B_2\cosh(\beta x) + B_3\sin(\beta x) + B_4\cos(\beta x). \end{aligned} \tag{2.36}$$

Using the same boundary conditions (se expressions (2.19) and (2.21)), and requiring the corresponding determinant of the homogenous linear system of equations for the constants, it is possible to numerically determine the frequencies of

the first modes. This can in turn be used to, similar to that for the freestanding case in expression (2.35), find an approximate expression fitted to the numerical solution

$$m_{eff} = m + \left(0.270 \left(\frac{h}{H} \right)^4 - 0.267 \left(\frac{h}{H} \right)^2 + 0.246 \right) m_{tower}, \tag{2.37}$$

which, when replacing m in expression (2.24), matches the full numerical solution based on (2.36), within a maximum eigenfrequency error of 1% for all h/H ratios. It can also be noted that, if neglecting the distributed tower mass, the error in eigenfrequency will be within 13-20%.

3. Method

3.1 Turbulence influence on wind energy extraction measurements

To investigate the influence of turbulence on the wind energy extraction of the T1-turbine, 1030 hours of operational data (excluding data rejected according to "3.1.2.6 Data rejection") from periods of automatic mode operation between June 2011 and August 2012 are studied.

3.1.1 Data collection setup

In addition to the T1-turbine, the experimental setup consists of a control system and the wind measurement mast. The measurements were logged, at a sampling frequency of 1 Hz, on the same CompactRIO (NI cRIO9074) used for the control system of the turbine. The DC power was measured with a SSET CEIZ04-55E4-1.0/0-400A current transducer and a Tektronix P5200 voltage transducer. The rotational speed of the turbine was measured by a 10-bit rotational encoder placed on the lower end of the drive shaft.

3.1.1.1 Meteorological measurements

The wind speed was measured by a Thies Clima 4.3351.00.161 cup anemometer, placed at a height of 42 m on a wind measurement mast situated 120 m from the actual turbine. The anemometer has an accuracy of < 1% or < 0.2 m/s. The signals from the anemometer are measured by a PLC and logged by one of the cRIOs of the wind turbine control system.

Air pressure and temperature were retrieved from the Swedish Meteorological and Hydrological Institute (SMHI). The temperature was retrieved as hour values from Hanarp (56°51'45.1"N 12°39'46.1"E) situated 12 km south-east of the T1-turbine. The air pressure was retrieved as hour values from Torup (56°56'58.6"N 13°3'45.0"E) situated 33 km to the east of the T1-turbine, and then recalculated to the elevation of the rotor centrum of the T1-turbine. For the measurements, the air temperature ranged between -10.9°C and 27.3°C and the air pressure ranged between 0.98 bar and 1.04 bar. Inserting the temperature and pressure values into equation (3.8), the air density ranged between 1.16-1.38 kg/m^3.

3.1.2 Data acquisition and treatment

When quantifying the performance of a wind turbine, the international standard for power performance measurements of wind turbines, "Wind turbines – Part 12-1: Power performance measurements of electricity producing wind turbines" IEC61400-12-1 [75], is usually followed. This implies using the mean wind speed over a period of 10 min when analyzing the relation between wind speed and performance. Since this method ignores the cubic effect (see "2.1 Turbulence and wind energy conversion"), higher wind variation leads to an overestimation of power curves and power coefficient curves in the lower wind speed range. Consequently, another approach than the standard must be used when investigating the relation between turbulence and performance. To be able to compare with earlier work regarding how turbulence affects power curves of HAWTs, as well as analyzing how it influences the performance of the VAWT considered in this work, two different approaches were used to retrieve power curves and power coefficient curves. Approach A, which in line with the IEC standard, ignores the cubic effect and approach B, taking the cubic effect into account, allowing comparing the turbine's performance for different turbulence intensities.

As mentioned, all data from the turbine and the adjacent wind measuring mast was logged at a rate of 1 Hz. Air pressure and temperature were retrieved as 1 hour values. Matlab was then used for further analysis of all values.

3.1.2.1 Approach A

If considering how the influence of the cubic effect is treated, approach A is consistent with IEC61400-12-1 and uses the 10 min mean values for wind speed in equation (2.1). This wind speed mean value is simply calculated by

$$\bar{v} = \frac{1}{N}\sum_{i=1}^{N} v_i, \tag{3.1}$$

where v_i is the 1Hz wind speed value and N is the number of values. Hence, the mean aerodynamic power coefficient is calculated as

$$C_p = \frac{\overline{P_{aero}}}{\left(\frac{1}{2}\rho A \bar{v}^3\right)}, \tag{3.2}$$

with the mean extracted aerodynamic power $\overline{P_{aero}}$ calculated by equation (2.3) and averaged over the same relevant time period as the mean wind speed $\bar{v}$. Since the turbulence influence on the energy content of a certain mean wind speed is not accounted for, approach A will, for the wind speeds of interest in this work, lead to an overestimation of both power coefficient and the power curve, which is shifted to the left with higher TI.

A difference compared to the IEC61400-12-1 standard, regarding power and power coefficient, is that here the aerodynamic power P_{aero} is considered rather than the electric power P_{el} as instructed in the standard.

The mean tip-speed ratio used for $C_p(\lambda)$ curves is calculated as

$$\bar{\lambda} = \frac{\bar{\omega}R}{\bar{v}}, \tag{3.3}$$

where $\bar{v}$ and $\bar{\omega}$ is the mean wind speed and mean angular velocity over the relevant time period.

3.1.2.2 Approach B

When comparing C_p to TI, it is of necessity to eliminate the effect of the cubic factor so that relations can be assumed to come from the actual behavior of the wind turbine. Since the power of the wind changes with the wind cube, the mean of the wind cube will hold the same amount of energy irrespective of TI. Similar approaches have been adopted previously in the same context. In [76], for example, the average wind energy flux (proportional to $\overline{v^3}$), i.e. the total amount of kinetic wind that passes an unit cross-section area per unit time, is used when retrieving an equivalent wind speed taking both wind speed and wind shear into account. The wind energy flux for a given time period is the same as the mean wind cube and in [76], it is calculated from the mean wind and turbulence intensity of that period. If, as in the case here, the data is logged at a high enough frequency, the mean wind cube can with the same result be retrieved from averaging the wind cube values. Therefore, in the second approach, the mean wind cube is used instead of the mean wind speed when calculating the aerodynamic power coefficient, in this version called $\widetilde{C_p}$. The mean wind cube $\overline{v^3}$ and $\widetilde{C_p}$ is obtained respectively according to

$$\overline{v^3} = \frac{1}{N}\sum_{i=1}^{N} v_i^3, \tag{3.4}$$

$$\widetilde{C_p} = \frac{\overline{P_{aero}}}{\left(\frac{1}{2}\rho A\overline{v^3}\right)}. \tag{3.5}$$

When using a power – wind speed relation, i.e. a power curve, to study how TI affects the turbine's energy extraction, it is also preferable to use $\overline{v^3}$ rather than $\bar{v}$. This again because the mean wind cube is directly proportional to the power of the wind, thus enabling displaying differences between different TIs without the cubic effect interfering.

3.1.2.3 Method of bins

As recommended in IEC61400-12-1, the method of bins has been used to analyze the measured data. The measured data, presented as 10 min mean values and for

some cases 1 min mean values, are divided into bins, i.e. equally sized sections depending on the value along the x-axis. After that, the mean values of the x-axis variable and the y-axis variable are calculated as

$$x_i = \frac{1}{N_i}\sum_{j=1}^{N_i} x_{i,j}, \tag{3.6}$$

$$y_i = \frac{1}{N_i}\sum_{j=1}^{N_i} y_{i,j}, \tag{3.7}$$

where $x_{i,j}$ and $y_{i,j}$ are the variables of data set j in bin i and N_i is the number of data sets in bin i. The averaged values of x_i and y_i can then be used to create a curve which represents the relation between the variables.

3.1.2.4 Normalization due to air density

The air density increases with air pressure and decreases with temperature, typically peaking during the winter season. To be able to compare the turbine's true ability for extracting wind energy at different air pressures and temperatures, each 10 min measurement period is normalized by accounting for changes in the air density. In equation (2.1), the air density for the period can be calculated by

$$\rho_{10\,min} = \frac{B_{10\,min}}{R_0 T_{air,10\,min}}, \tag{3.8}$$

where $B_{10\ min}$ and $T_{air,10\ min}$ are the measured air pressure and temperature for the specific 10 min period and R_0 is the gas constant (287.05 J/(kg K) for air) [75]. When calculating C_p, the normalization is incorporated straightforwardly as the current air density is used in equations (3.2) or (3.5). For power curves, the normalization is done by adjusting the power output according to

$$P_n = P_{10\,min}\frac{\rho_0}{\rho_{10\,min}}, \tag{3.9}$$

where P_n is the normalized power output, $P_{10\ min}$ is the measured power averaged over 10 minutes and ρ_o is the reference air density, here set to the ISO standard atmosphere of 1.225 kg/m^3 [75]. Since the aerodynamic performance of the turbine (i.e. wind energy to torque) is the main interest of this work, $P_{10\ min}$ is averaged from the P_{aero} values.

3.1.2.5 Normalization due to driveline efficiency

The driveline efficiency of a wind turbine can vary quite extensively depending on operating conditions and to be able to compare the turbine's aerodynamic performance, this efficiency needs to be accounted for. In this work, normalization

for a varying driveline efficiency is implemented for each 1Hz measurement value when calculating P_{aero} (and thus also C_p). The driveline efficiency is retrieved from

$$\eta_d = \eta_g \eta_m, \tag{3.10}$$

where η_g is the generator efficiency and η_m is the mechanical efficiency, handling for example couplings and bearings. Here, the driveline efficiency η_d is the relation between the aerodynamic power converted by the rotor and the measured DC power, hence the efficiency of the DC/AC-converter does not need to be accounted for. The T1-turbine's generator efficiency η_g used in equation (3.10) is found from simulations and presented in [77]. As an approximation, the mechanical losses of the T1-turbine is estimated to be equivalent to an efficiency of 0.99 at full power and maximum rpm and then set to vary linearly with the rotational speed. For the operational conditions of this work, η_d will mainly be found within 0.70-0.95 with a mean of 0.85.

3.1.2.6 Data rejection

Samples containing start or stop routines have been rejected. As low power data may magnify eventual measurement errors, samples with a mean power less than the approximate cut-in threshold of 5 kW has also been rejected. Sequences when the turbine was not operating in its normal routine, for example when testing or tuning the control system, were also rejected.

3.2 Noise measurement campaigns

To investigate the noise characteristics of the T1-turbine, two separate noise measurement campaigns have been performed: one noise emission measurement to evaluate the noise levels and one microphone array measurement aiming to localize aerodynamic noise sources.

3.2.1 Noise emission measurements

3.2.1.1 Experimental setup

The microphone used was a BSWA MP201 which together with preamplifier MA211 gives a flat frequency response and Class 1 accuracy (< 0.7 dBA) according to the international standard for sound level meters, IEC61672-1 [78]. A Norsonic Nor140 was used as field recorder. For calibration, an acoustic calibrator, Brüel & Kjær type 4231, was used. For setting the distance to the tower, a laser rangefinder, Leica Pinmaster, with an accuracy of ±1m, was used.

For recording the sound pressure level of the wind turbine, the microphone was mounted on an acoustically hard circular board with a primary 90 mm and a secondary 250 mm wind protection. The circular board gives a coherent addition b = 6 dB. The total acoustic attenuation of the wind protections is 0.5 dB with the largest

effect on higher frequencies, this effect is deemed negligible and has not been accounted for in the result. The entire setup is consistent with the IEC61400-11 standard.

The wind speed and rotational speed of the turbine was measured according to "3.1.1 Data collection setup".

3.2.1.2 Observations

The T1-turbine is situated in a plain field with a freeway with heavy traffic 750 m to its southwest. Interfering noise from this freeway was evened out due to the distance and was approximately at the same level during the entire recording. Furthermore, there is a farm located nearby with its access road just 70 m from the turbine but there were no interfering traffic during the time of recording. The microphone was placed at a distance of 40 m downwind from the tower base and a recording was performed with the turbine first turned on for 60 minutes, then turned off for 24 minutes and then turned on again for another 11 minutes.

The measurements were performed between 09:00 and 10:30, on 2012-03-07. The mean wind speed at hub height during the measurements was 8.0 m/s and 9.5 m/s with the turbine turned on and off respectively. If recalculated to the standard 10 m height, using a power-law wind profile with exponent 0.17, these wind speeds equals 6.3 m/s and 7.4 m/s.

3.2.1.3 Binning values and standard uncertainty

When using equations (2.13) and (2.14) to calculate the noise emission for a certain wind speed, $L_{p,rec}$ and $L_{p,bg}$ must be quantified for that wind speed. For this, the IEC standard specifies using the method of bins which has been previously described in "3.1.2.3 Method of bins". For this case, 10 s mean values are used for sound pressure levels and wind speed respectively. Binning the wind speed into the mean wind speed $\bar{V}_i$ is straightforward but for the case of sound pressure levels L_p, values must first be transformed to squared sound pressure p^2 (see equation (2.8)) before averaging to bins and allowing calculating the equivalent sound pressure level $\bar{L}_{p,i}$ for bin *i* according to

$$\bar{L}_{p,i} = 10\log_{10}\left(\frac{1}{N_i}\sum_{j=1}^{N_i} 10^{\left(\frac{L_{p,i,j}}{10}\right)}\right), \tag{3.11}$$

where $L_{p,i,j}$ is the sound pressure level at measurement period *j* in bin *i*, and N_i is the number of measurement periods. The sound pressure level at wind speeds not coinciding with $\bar{V}_i$ is obtained by linear interpolation of the mean bin values. Doing this for both $L_{p,rec}$ and $L_{p,bg}$ for a certain wind speed, $L_{p,wt}$ (and thereby also $L_{W,wt}$) can be calculated for that wind speed.

The calculation of the standard uncertainties follows the prescription in the IEC standard. The standard uncertainty for $\bar{L}_{p,i}$ is calculated as

$$u_{L_{pi}} = \sqrt{\frac{{\sigma_{L_{pi}}}^2}{N_i} + {u_{L_{pe}}}^2}, \tag{3.12}$$

where $\sigma_{L_{pi}}$ is the standard deviation of $\bar{L}_{p,i}$ for bin i, and $u_{L_{pe}}$ is the overall precision of the corresponding measurement equipment. The next step is to obtain the standard uncertainties at the interpolated positions, for which the uncertainty of the wind speed is also needed (calculated analogously to equation (3.12)), as well as the covariance of the wind speed and the sound pressure level. See [63] for details.

3.2.1.4 Measurement limitations

According to the IEC61400-11 standard, regarding VAWTs, a distance $R_h = H + D$ should be used between the measuring position and the turbine, where H is the hub height and D is the rotor diameter. A 20% or maximum 30 m deviation is allowed as long as the distance is measured with an accuracy of ±2%. However, in this study a distance $R_h = H$ was used which is below the minimum distance allowed for VAWTs. The distance $R_h = H + D$ appears reasonable for guy-wired Darrieus-type VAWTs (the historically most common type), where hub heights are generally low. The specified HAWT distance, $R_h = H + D/2$, would in the Darrius case imply a measurement point very close to the blade. The VAWT studied here, with its high tower, is in this sense however more similar to a HAWT. In addition, the relatively high noise level due to the nearby freeway motivated a measurement point even a little closer, at $R_h = H$, to increase signal-to-noise ratio.

The measurements were performed with an upper limit of the rotational speed set to 22 rpm (the reason for this is described in "1.1.3 The 200-kW T1-turbine"). The limitation means that the turbine was operated at target tip speed for the measurements done at 6 m/s (10 m height) but for higher wind speeds the tip speed was below target and thus the turbine was stalling. The stalling contributes to the creation of noise while the lower velocity of the blade counteracts it [48]. It is unclear which effect is most important.

3.2.2 Microphone array measurements

3.2.2.1 Experimental setup

The microphone array is built up of 48 microphones positioned along six spiral arms making up a total array diameter of approximately 1.5 m, the array can be seen in Figure 3.1. Microphone positions have been calculated with the help of the equation for Fermat's spiral, resulting in an irregular microphone configuration (as opposed to a periodic one, e.g. a rectangular grid). Similar multiple-spiral-arm patterns has been observed to produce high side-lobe suppression [79].

Class 1 BSWA 1/4" phase-matched array microphones were used. Microphone signals were recorded with two synchronized Alesis HD24 hard-disc recorders, at the sampling rate 44100 Hz.

The wind speed and rotational speed of the turbine as well as the metrological conditions was measured according to “3.1.1 Data collection setup”.

Figure 3.1: The microphone array used throughout this work. The array is built up of 48 microphones in a spiral pattern.

3.2.2.2 Observations

Recordings were performed at four positions, all at the same distance of 39.5 m from the turbine center but at different directions, for all cases the array was directed towards the top of the tower. In Table 3.1, corresponding wind directions (measurement angles), wind speeds and ambient turbulence intensities for all four positions can be seen.

The measurements were performed between 22:30 and 23:30, on 2015-06-15, the late hour was chosen to minimize interfering noise from the nearby freeway. The wind direction was close to western. The turbine was operating at the lower limit rotational speed, staying within 15.8-16.2 rpm during the entire operational time. The humidity was just above 100%, the temperature was around 11°C and the air pressure was steady at 1.015 bar during the entire measurement.

Table 3.1: *Wind speed, corresponding wind direction, and measured atmospheric turbulence intensity for the measurement positions. The measurement angles between the measurement position and the wind direction counted counterclockwise from downwind (positions marked out in Figure 4.11). The 10 m wind-speed values are calculated from the hub height values, using a power-law wind profile with exponent 0.17.*

Position	Wind speed at hub height (m/s)	Wind speed at 10 m (m/s)	Measurement angle (°)	Turbulence intensity (%)
1	4.7	3.7	31	20
2	6.0	4.7	126	11
3	5.4	4.2	218	12
4	5.0	3.9	303	13

3.2.2.3 Data processing

Each recording took about 20 s, representing about five revolutions of the rotor blades. The calculated source maps represent the average sound radiation during these five laps. Source maps were generated using Acoular software [80, 81] with basic delay-and-sum algorithm in the frequency domain and diagonal deletion to remove wind-generated microphone noise. Diagonal deletion also reduced adverse effects of background noise from the nearby freeway, which might be explained by loss of coherence as the sources are distant and obscured by elevations in the landscape, forcing the sound to travel along different paths [65]. A subsequent DAMAS [64] deconvolution removed side-lobe effects and improved image resolution. Sound-pressure-level spectra and turbine sound-pressure levels were produced by integrating over the source maps.

3.3 Eigenfrequency measurements and simulations

Measurements and simulations on the fist-mode eigenfrequency of the semi-guy-wired tower are performed to evaluate the derived expressions in ”2.3 Eigenfrequencies of the semi-guy-wired tower”.

An inclinometer SCA121T-D03 placed at the top of the tower (and part of the turbine’s active monitoring system) was used for g-force measurements. The analog signal was logged in 100 Hz and then treated in MATLAB for Fast Fourier Transform (FFT) analysis.

Finite Element Method (FEM) simulations for eigenfrequencies of the tower were carried out using SolidWorks Simulation. Several models were simulated to evaluate the different means for choosing second moment of area and tower mass as described in “2.3.3 Effective spring constant, second moment of area and tower mass”. These simulated models are further described in “4.3.1.1 Simulation of tower eigenfrequency”.

4. Results and discussion

4.1 Turbulence influence on wind energy extraction

The influence from turbulence on the wind energy extraction is studied by evaluating logged operational data from the measurements described in "3.1 Turbulence influence on wind energy extraction measurements".

4.1.1 Turbulence influence on power curves and power coefficient

To the left in Figure 4.1, the power curve of the T1-turbine can be seen. It is made according to approach A (see "3.1.2.1 Approach A"), based on 10 min mean values and for each bin (see "3.1.2.3 Method of bins") the standard deviation of its power values is plotted. Also in Figure 4.1 (center and right), power curves for values categorized depending on turbulence intensity (TI, from equation (2.5)) are plotted. Similarly, but according to approach B (see "3.1.2.2 Approach B"), in Figure 4.2, the power is plotted against the mean wind cube $\overline{v^3}$ so that different turbulence intensities can be compared without accounting for the difference in available energy for a given mean wind speed. In Figure 4.1, it can be seen that higher turbulence intensity gives more power. However, part of this is due to the higher level of wind energy for a given mean wind speed that comes with a higher turbulence intensity. This becomes evident as the influence from turbulence intensity is weaker in Figure 4.2, although also here TI is positively connected to power for most wind speeds. Since a certain mean wind cube holds the same amount of wind energy irrespectively of TI, this indicates that the T1-turbine is, somewhat unexpectedly, more efficient at higher TI.

In Figure 4.3, $\widetilde{C_p}$ is plotted against turbulence intensity, both as 10 min mean values and 1 min mean values. Consistent with approach B, the mean wind cube is used when calculating $\widetilde{C_p}$, thereby accounting for the cubic effect. For both plots, $\widetilde{C_p}$ increases with TI, once more indicating that the T1-turbine is more efficient at turbulent conditions. The $\widetilde{C_p}$ –TI relation is stronger with 1 min mean values, which could be expected as longer-term wind variations will have more influence on the 10 min values, diluting any relation between turbulence and energy extraction.

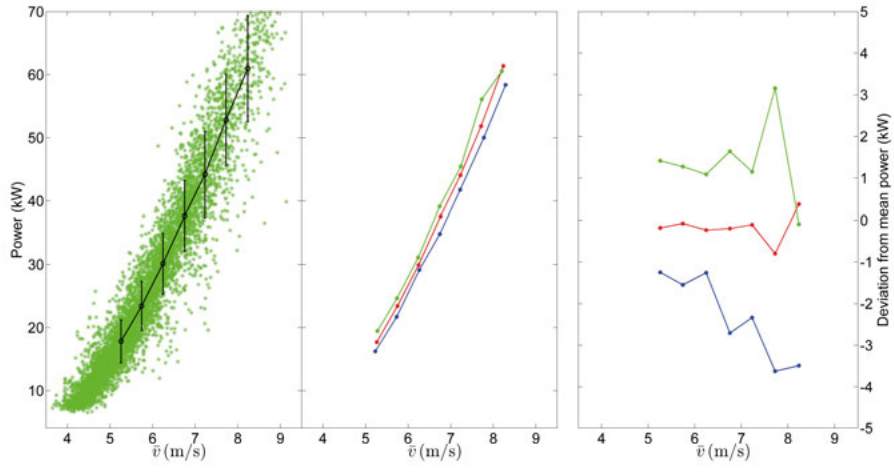

Figure 4.1: Consistent with approach A: Power (P_{aero}) curve with mean values and standard deviation for each bin (left in figure), curves divided by TI with mean values for each bin (center). To the right, the TI-divided curves are presented as deviation from mean power for each bin. Blue: Low TI (< 10%), Red: Medium TI (10% < TI < 15%), Green: High TI (> 15%).

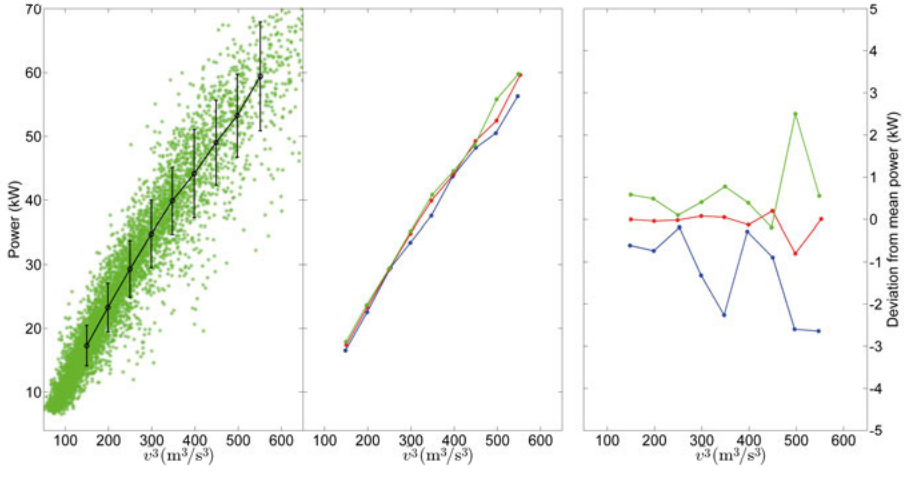

Figure 4.2: Consistent with approach B: Power (P_{aero}) as a function of mean wind cube with mean values and standard deviation for each bin (left in figure), curves divided by TI with mean values for each bin (center). To the right, the TI-divided curves are presented as deviation from mean power for each bin. Blue: Low TI (< 10%), Red: Medium TI (10% < TI < 15%), Green: High TI (> 15%).

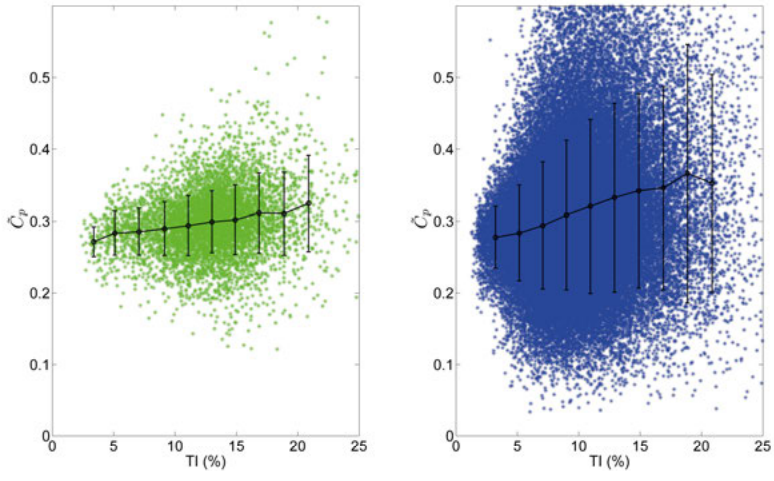

Figure 4.3: Turbulence intensity influence on $\tilde{C}_p$ from 10 min mean values (left) and 1 min mean values (right).

In [40], turbulence influence on a standardized power curve for an unspecified HAWT is presented and in [42, 43] equivalent curves are simulated. The power-TI relation resembles that in Figure 4.1, higher TI gives more power. As earlier mentioned, this difference for a standardized curve (approach A) is mainly due to the cubic effect which aggravates the comparison.

In [47], a figure resembling Figure 4.2 is presented for a modern multi-MW HAWT, showing very small differences in power for TI < 10% and TI > 13%. However, the nacelle cup anemometer was used for wind measurements which may influence the result. Within the same article, equivalent results with SODAR measurements are also presented, indicating a clear negative dependency for power with TI. For both cases, the effect from wind shear on the representable rotor area wind speed was accounted for. In Figure 4.2, without accounting for wind shear, TI has a small positive influence on power within almost the entire wind cube range. A SODAR or LIDAR measurement of the TI for the present situation would probably show higher TI (as indicated by the measurements in [47]), which would lead to larger mean wind cube values for the same power, and therefore it is likely that the positive trend would disappear. Still, as the cup anemometer results do not show a positive trend in [47], as they do here, the present results indicate that VAWTs are more positively influenced by turbulence than HAWTs.

The T1-turbine's seemingly good ability to extract wind energy at high turbulence can partly be explained by the fact that VAWTs are omni-directional. Since more turbulence also will increase the alternation rate in wind directivity, this gives the VAWT an advantage over HAWTs. Changes in wind direction can also have a positive effect for the power production, as the wake will be shed in different direction, which can lower the blocking effect of the wake, hence slightly increasing the flow velocity at the turbine.

As earlier mentioned, [47] emphasize the importance of TIs relation to convective atmospheric conditions and low wind shear. The difference between the mean hub-height wind speed and the effective mean wind speed will be even more pronounced for a vertical-axis wind turbine as the rotor cross-section area is rectangular. The difference could be positive or negative depending on meteorological conditions, and this makes it more difficult to know exactly the expected effect of TI upon power production, since we have no data on wind shear and atmospheric stability here.

4.1.2 Turbulence influence on optimum tip-speed ratio

Interesting in itself (although at first sight not on the turbulence topic), in Figure 4.4, the experimental $C_p(\lambda)$ curve of the T1-turbine is displayed, indicating a maximum C_p of 0.33 at a λ of 4.3. Consistent with the IEC61400-12-1 standard, 10 min mean values are used and C_p is calculated according to approach A. The standard deviation of the C_p values for each bin has also been plotted. As a comparison, a 12-kW VAWT prototype of the same concept as the T1-turbine has been shown to have a maximum C_p of 0.29 at a λ of 3.3 [82].

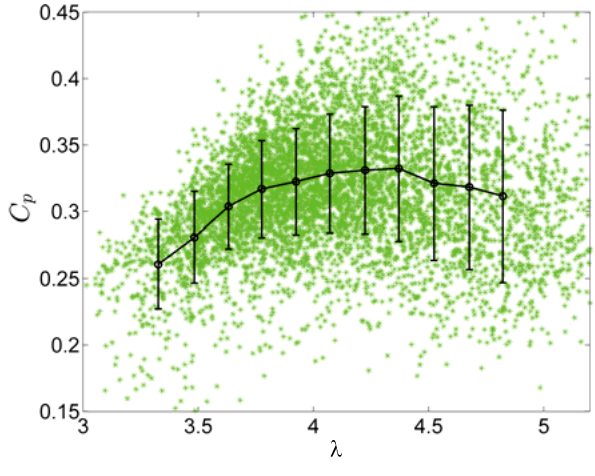

Figure 4.4: Experimental $C_p(\lambda)$ curve (black) made from binned 10 min mean values (green).

By producing several $C_p(\lambda)$ curves, each one representing a different TI span, the influence of turbulence on the optimum tip-speed ratio $\lambda_{C_{p-max}}$ can be examined. This is done in Figure 4.5, where third grade curves are fitted to the bin means so that the maximum C_p value and thus $\lambda_{C_{p-max}}$ can be found. This results in a plot relating TI to $\lambda_{C_{p-max}}$, seen in Figure 4.6. These figures display a clear positive dependence between TI and $\lambda_{C_{p-max}}$. Within TI of 6-16%; there is an approximate increase of 0.1 in $\lambda_{C_{p-max}}$ for every 5% raise of TI. For 16-20%; there is an even stronger relation; however, the results from this span are more uncertain as it has larger standard deviations and somewhat uneven distribution of mean C_p values.

With exception of the highest TI span of 16-20% in Figure 4.5, the fitted curves nearly intersect all mean C_p values which adds reliability to the results. In Table 4.1, $\lambda_{C_{p-max}}$, mean TI, mean wind speed, mean λ and number of 10 min samples can be seen for each TI interval.

The possible gain in C_p from setting the control strategy so that λ varies with TI according to Figure 4.6 can be estimated. This by, for each TI interval in Figure 4.5, comparing the maximum C_p-value from the fitted curves with the C_p-value that is obtained using the fixed $\lambda_{C_{p-max}}$ (from Figure 4.4). The average gain in C_p for all TI intervals, weighted for the TI distribution, is found to be 0.6% (counted as relative percentage). The gain for each TI interval can be seen in Table 4.1, with the highest value (2.5%) found for the highest TI interval and the second highest value (0.7%) found for the lowest TI interval. For the mid-range TI intervals, the magnitude of the power coefficient gain is close to zero which is natural as the $\lambda_{C_{p-max}}$ for these intervals are close to the fixed TI-independent $\lambda_{C_{p-max}}$.

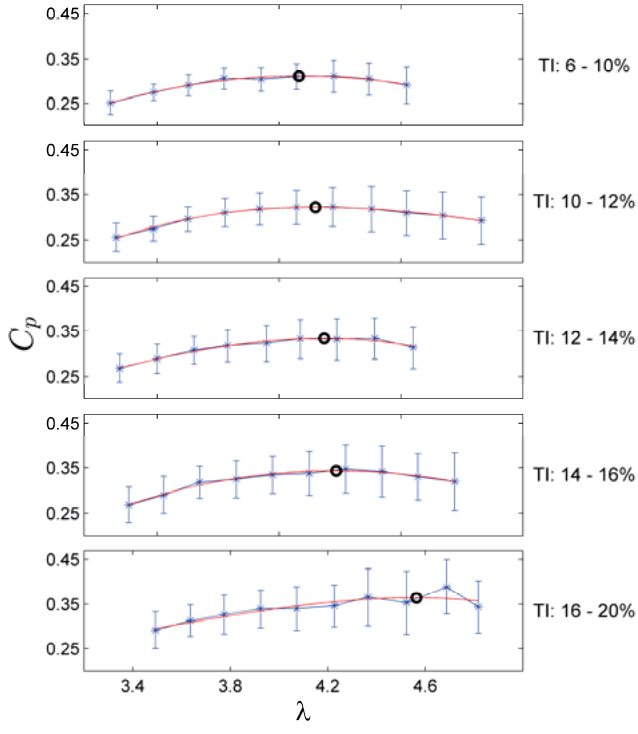

Figure 4.5: $C_p(\lambda)$ curves for different TI with standard deviation (blue), fitted curves (red) and maximum value (at $\lambda_{C_{p-max}}$) indicated with a black circle.

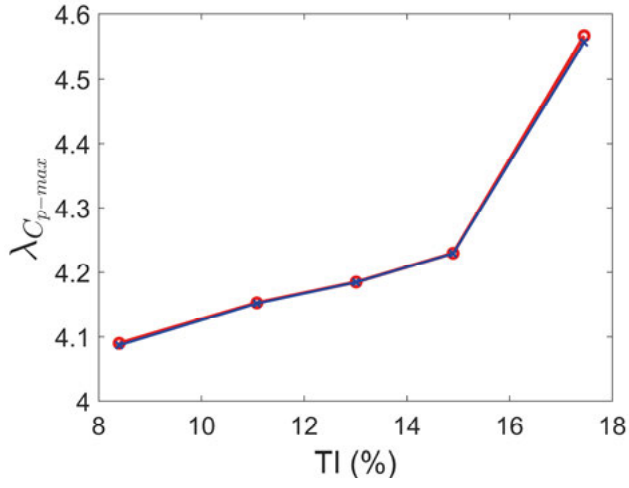

Figure 4.6: Relation between $\lambda_{C_{p-max}}$ and TI from $C_p(\lambda)$ curves according to "3.1.2.1 Approach A" (blue) and $\widetilde{C_p}(\lambda)$ curves"3.1.2.2 Approach B" (red). The upper right point is coupled to larger uncertainty due to anomalies in the high turbulence data (see Figure 4.5).

Table 4.1: $\boldsymbol{\lambda_{C_{P-max}}}$ *and various specifications for each TI span.*

TI (%)	Mean TI	$\lambda_{C_{P-max}}$	Mean λ	Mean wind speed (m/s)	No of 10 min samples	Possible gain of C_p (rel %)
6-10	8.40	4.08	4.24	5.66	913	0.7
10-12	11.08	4.15	4.09	6.03	1117	0.2
12-14	13.01	4.19	4.18	6.12	1508	0.1
14-16	14.90	4.23	4.09	6.13	1284	0.0
16-20	17.45	4.56	4.16	5.91	943	2.5

As mentioned earlier, the cubic effect leads to an overestimation of C_p with higher TI. However, this does not seem to be linked to the tip-speed ratio and thus does not affect the comparison of $\lambda_{C_{p-max}}$ for each different TI span. This can be seen in Figure 4.7 with two sets of $C_p(\lambda)$ curves for different TI, one set with C_p according to approach A (see "3.1.2.1 Approach A") and one set with $\widetilde{C_p}$ according to approach B (see "3.1.2.2 Approach B"). The $\widetilde{C_P}$ curves are, as could be expected, more pushed together than the C_p curves. However, the relation between TI and $\lambda_{C_{p-max}}$ are the same for both cases which is displayed in Figure 4.6 where $\lambda_{C_{p-max}}$-TI relation can be seen to be almost independent on which of the two methods that is used. Additionally, it could be suspected that the shift in $\lambda_{C_{p-max}}$ upwards derives from a secondary effect linked to the turbulence rather than the turbulence itself. Most likely to interfere is the wind speed which is linked to the Reynolds number and thus could affect $\lambda_{C_{p-max}}$ [83]. However, as can be seen in Figure 4.8, there is no strong linkage between TI and the wind speed, so the main shift in $\lambda_{C_{p-max}}$ can be assumed to come from the turbulence.

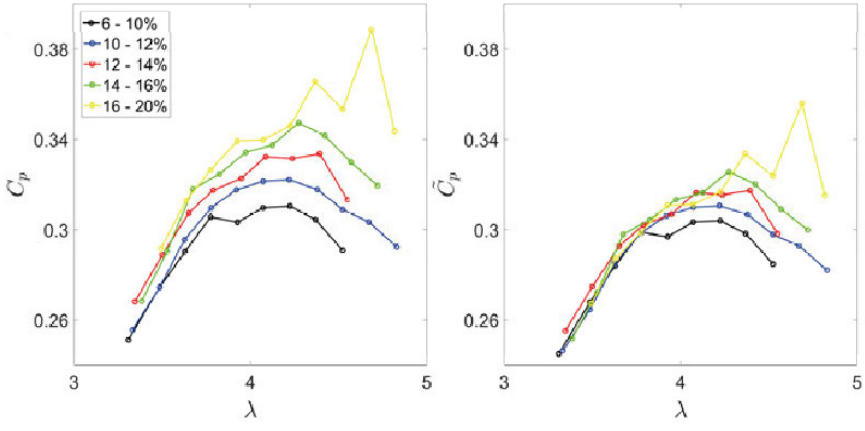

Figure 4.7: $C_p(\lambda)$ curve for different TI with C_p from mean wind according to "3.1.2.1 Approach A" (left) and $\widetilde{C_p}$ from mean wind cube according to"3.1.2.2 Approach B" (right).

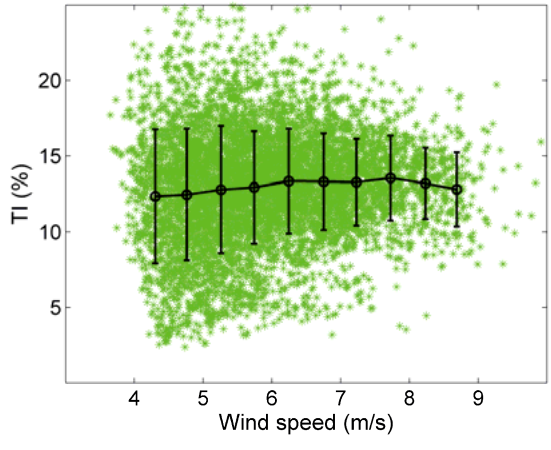

Figure 4.8: The relation between TI and wind speed (black) with the standard deviation for TI of each bin, made from binned 10 min mean values (green).

The demonstrated increase of $\lambda_{C_{p-max}}$ with TI can partly be explained by the fact that a higher tip-speed ratio raises the potential for extracting the energy-rich wind gusts. The cubic variation of power with wind speed makes it more beneficial with a higher $\lambda_{C_{p-max}}$ as the efficiency gain with the high-energy wind gusts is greater than the efficiency loss with the lower energy dips in wind speed. This is also illustrated by the indication that the largest potential for improvement is found at the highest TIs, where an increase of λ leads to a higher C_p. Also interesting is that there is potential for improvement for the lowest TIs, where a decrease of λ leads to a higher C_p.

4.2 Noise from VAWTs

Here, the results from the two noise measurement campaigns described in "3.2 Noise measurement campaigns" are presented, followed by comparisons to the noise models described in "2.2.1 Aerodynamic noise prediction models".

4.2.1 Noise emission measurements

As mentioned in "3.2.1.2 Observations", a recording was performed with the turbine turned on and off sequentially. The 10 s based mean values are binned according to "3.2.1.3 Binning values and standard uncertainty" (assuming that the turbine is turned off when the electric output is below 5% of rated power). By this, the total and background noise, respectively, can be presented as functions of wind speed, see Figure 4.9. Using linear interpolation between the mean bin values from Figure 4.9, together with equation (2.13), the wind turbine sound pressure level $L_{p,wt}$ can be decided for different wind speeds. Thereafter, the noise emission $L_{W,wt}$ can be decided with equation (2.14). The noise emissions with standard uncertainty for wind speeds between 5 and 8 m/s are displayed in Table 4.2.

The noise emission of the T1-turbine at 8 m/s, 10 m above ground, was measured to 96.2 dBA. At this wind speed the turbine was stalling due to the upper limit of the rotational speed added after installing the guy wires, and the effect of this upon the noise level is unclear as there are two balancing effects (see "3.2.1.4 Measurement limitations"). The noise emission at 6 m/s, 10 m above ground, was measured to 94.1 dBA, this while operating at the target tip speed.

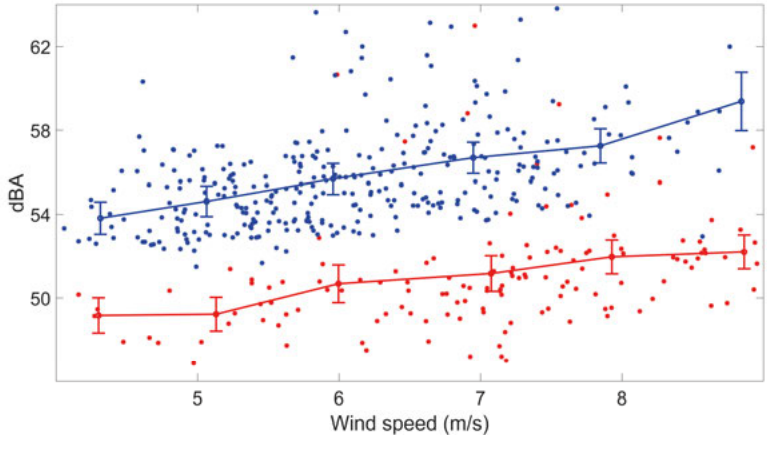

Figure 4.9: Sound pressure level against wind speed (recalculated to 10 m above ground) presented as 10 s mean values with turbine turned on (blue) and off (red). Binned mean values with standard uncertainty and linear relations between bin means for the sound pressure levels.

Table 4.2: *Noise emission for different wind speeds calculated from results of recordings.*

Wind speed at 10 m height	m/s	5	6	7	8
Tip-speed ratio		3.8	3.8	3.4	2.9
Noise emission	dBA	93.1	94.1	95.4	96.2
Noise emission standard uncertainty	dBA	±1.0	±1.1	±1.0	±1.0

4.2.1.1 Comparison with similar sized HAWTs

Available noise surveys performed on similar sized HAWTs [84-87] have established noise emissions of 95.1-100.2 dBA and 97.3-102.4 dBA for 6 and 8 m/s respectively, see Table 4.3 for details. Using this for comparison, the T1-turbine indicates a noise emission at the absolute lower range of the similar size HAWTs while running at target tip speed. At 8 m/s the noise emission of the T1-turbine is still lower than any of the compared HAWTs.

Table 4.3: *Noise emission and specifications of HAWTs in comparison. Wind speeds for noise emissions are stated for 10 m above ground [84-87].*

Turbine model	Power (kW)	Rotor diameter (m)	No of blades	Power reg.	dBA at 6 m/s	dBA at 8 m/s
Vestas V27	225	27	3	Pitch	96.7	97.3
GEV-MP R	200-275	32	2	Pitch	100.2	102.4
WTN250	250	30	3	Stall	95.1	99.8
Norwin 29/225	225	29	3	Stall	95.2	97.5

4.2.2 Microphone array measurements

Figure 4.10 shows 1/3-octave-bands source maps (microphone array images) from the measurement at position 2 (for positions, see Table 3.1 or Figure 4.11). It is evident that at low frequencies (around 800 Hz), the main noise source is located at a very specific azimuth angle of the blade. At higher frequencies the sources are distributed over a wider range of blade-azimuth angles, seemingly along the trajectories of the blade-strut joints, i.e. where the blade attach to the struts. Note that the upper limit of the color scale varies for the different bands in this image, the levels at low frequencies being considerably larger. The conformance between the distinct pattern of the higher-frequency source maps and the blade-strut-joint trajectory (see Figure 4.13) is used when mapping the scanning grid onto the turbine CAD-model image.

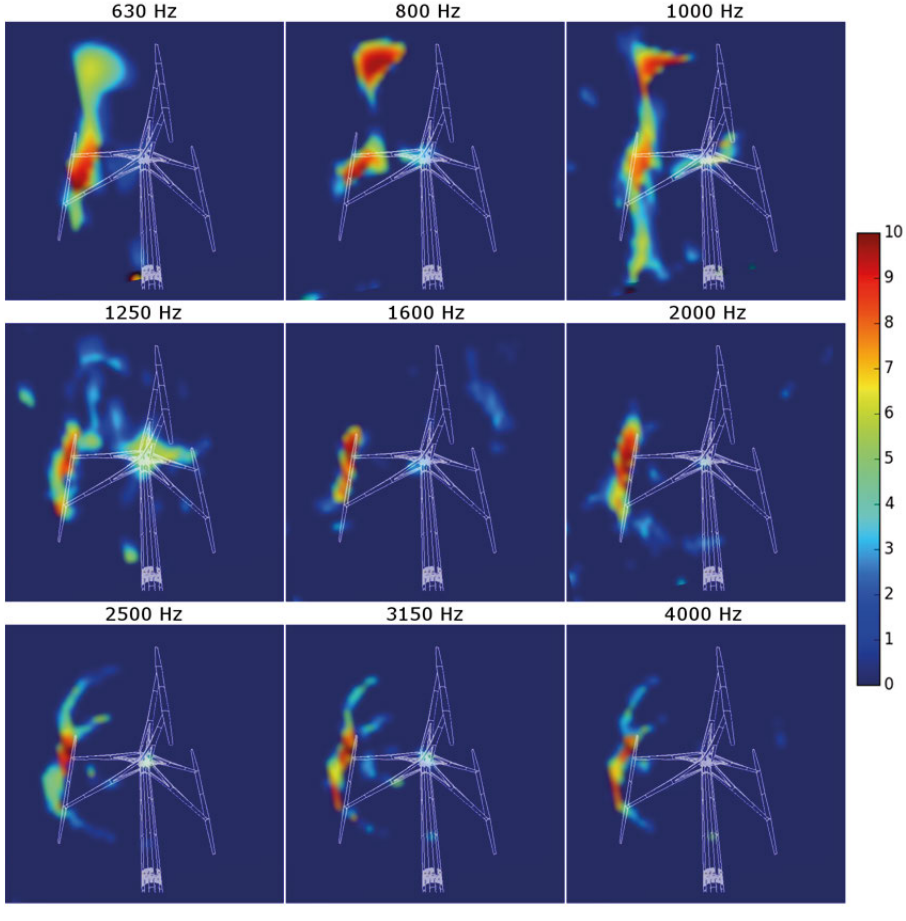

Figure 4.10: 1/3 Octave bands for position 2. Scale in relative dB. Scale upper limits are 17 dB (630 Hz), 16 dB (800 Hz), 10 dB (1000 Hz) (10 dB), 7.5 dB (1250 Hz), 5 dB (1600 Hz), 3 dB (2000 Hz), 3 dB (2500 Hz), 4.5 dB (3150 Hz) and 2 dB (4000 Hz).

For a comparison between the different measurement positions, Figure 4.12 and Figure 4.13 show octave band source maps at 800 Hz and 3150 Hz, respectively. The location of the noise sources seen in these figures is consistent between the positions. The lower-frequency source, for example, is located at the same azimuth angle with respect to the wind direction for all four positions. The azimuth angle can be extracted by comparing blade positions at different azimuth angles in a perspective-correct CAD model to the microphone array images, resulting in an azimuth angle of $\beta = 88°$ to the wind direction, see Figure 4.11. This is roughly the position where the relative wind speed is maximal, as the blade travels towards the flow.

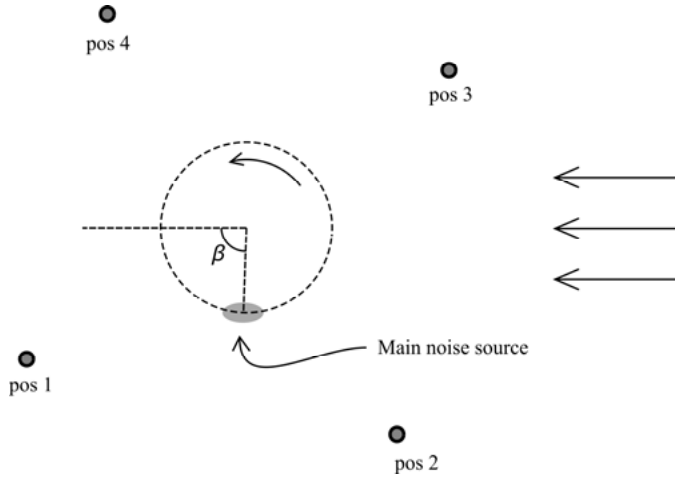

Figure 4.11: Measurement positions and the main (i.e. the lower-frequency) noise-source position, as seen from above (compare with Figure 4.12). The wind direction and the blade trajectory are also shown. The angle $\beta = 88°$ is the blade-azimuth angle (with respect to the wind direction) where the lower-frequency noise is emitted.

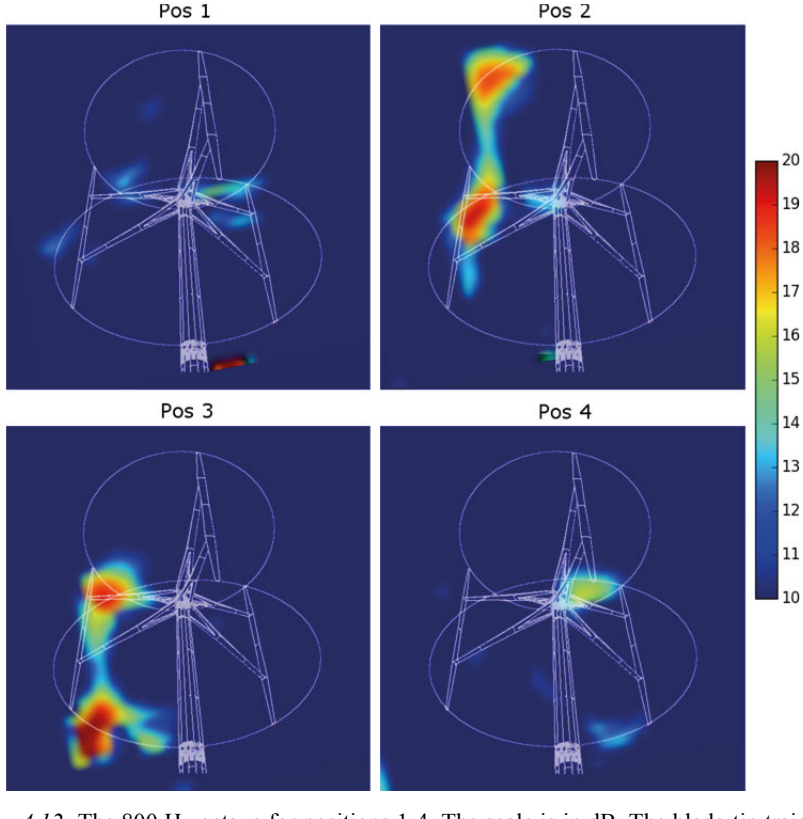

Figure 4.12: The 800 Hz octave for positions 1-4. The scale is in dB. The blade-tip trajectory is indicated in the figures.

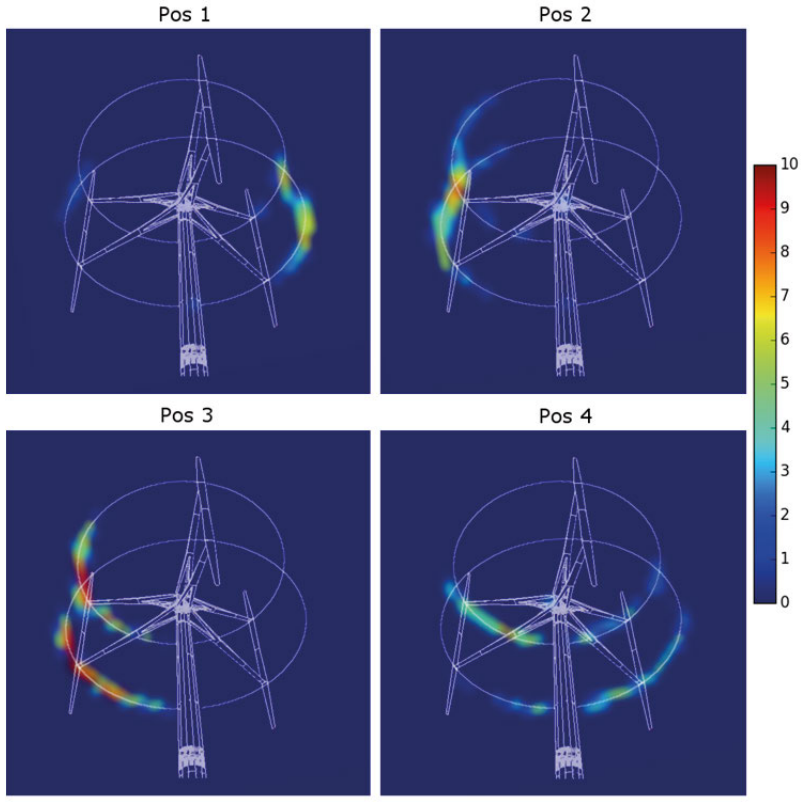

Figure 4.13: The 3150 Hz octave for positions 1-4. The scale is in dB. The blade-strut-joint trajectory is indicated in the figures.

4.2.3 Comparison with noise prediction models

To investigate which noise source is the most important for the T1-turbine, models for the TBL-TE and inflow-turbulence noise are compared with measured results from the noise emission and microphone array campaigns. The TBL-TE model (see "2.2.1.1 TBL-TE noise model") can be used relatively straightforwardly. The inflow-turbulence noise model in equation (2.9) can also be used as described in "2.2.1.2 Inflow-turbulence noise model", although some assumptions are necessary which are described in "2.2.1.3 Application of the inflow-turbulence noise model".

When comparing the measured results with the models for a certain recording position, the difference in directivity of the two noise contributions will alter the comparison depending on position. Therefore, the directivity of the two models must be considered before drawing conclusions. The directivities as well as marked out recording positions can be seen in Figure 4.14. Although most noise is emitted when the blade is moving towards the wind for both models, the inflow-turbulence model has a sharper directivity pattern which is due to the narrow region where the blade interact with self-induced turbulence (while noise is created more evenly during the entire revolution for the TBL-TE model). It can be observed that the dip in the noise

level from the inflow-turbulence model is at the position where the observer is standing in line with the emitting blade.

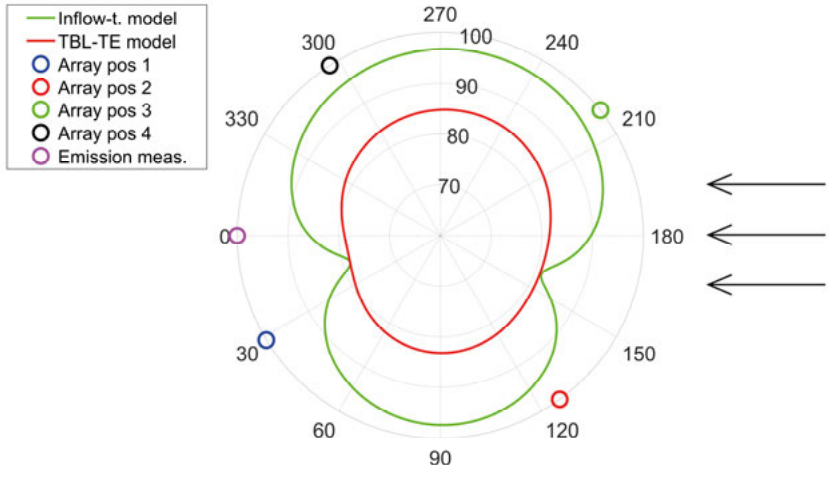

Figure 4.14: Directivity of the inflow-turbulence model (green) and TBL-TE model (red) as seen from above with the wind coming from the right. The comparison is for a distance of 40 m from the turbine base, a wind speed (hub height) of 8.0 m/s (6.3 m/s at 10 m height) and n=22 rpm. The positions (measurement angles) for microphone array measurements and noise emission measurement are marked in the figure. Units in dBA and degrees counted counterclockwise from downwind position.

4.2.3.1 Comparing models with the noise emission measurement

The noise emission measurement is compared to the models in Table 4.4 and Figure 4.15. In Table 4.4, the measured noise emission for wind speeds between 5 and 8 m/s (at 10 m height) is compared with the corresponding noise emissions from the models. Figure 4.15 show a comparison of the 1/3 octave bands of the turbine noise. For the case of the measurement, each of the bands is calculated using the same method as described for $L_{p,wt}$ in "4.2.1 Noise emission measurements". For both measurement and models, the bands correspond to the turbine sound pressure level, 40 m downwind from the tower base and a wind speed of 8.0 m/s (at hub height). For both the emission levels and 1/3 octave bands, it is clear that although the levels from both models are substantially lower than the measured levels, the inflow-turbulence model is far closer than the TBL-TE model. The still considerably lower levels of the inflow-turbulence model compared to the measured levels are best explained by a sharper directivity in the model than in reality (the downwind position is close to where the least noise is expected, see Figure 4.14).[11]

[11] This is seen in Figure 4.16, where the sound pressure levels of the inflow-turbulence model are slightly overestimated for position 2-4 (all where the inflow-turbulence model is close to maximum levels) while it is significantly underestimated for position 1 (close to minimum level of model).

Table 4.4: *Measured noise emission and equivalent model values (40 m downwind of the turbine).*

Wind speed at 10 m height (m/s)	5	6	7	8
Tip-speed ratio	3.8	3.8	3.4	2.9
Measurement (dBA)	93.1	94.1	95.4	96.2
TBL-TE model (dBA)	72.6	77.5	78.4	77.6
Inflow-turbulence model (dBA)	79.2	84.3	87.0	88.4

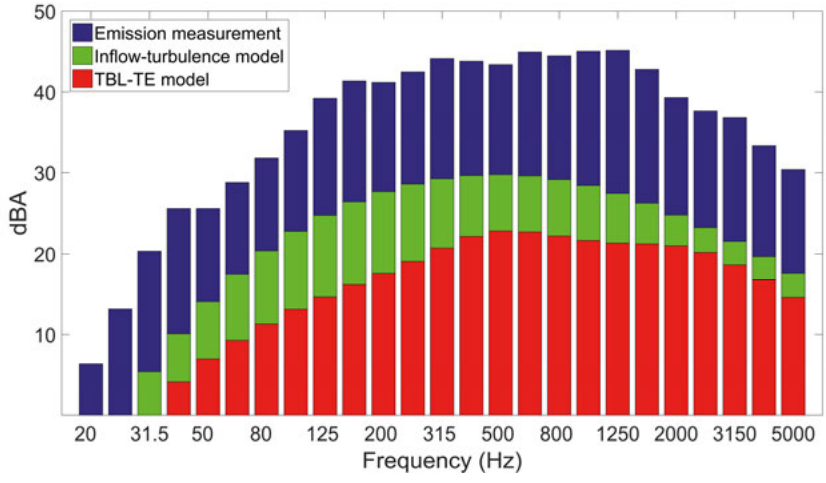

Figure 4.15: Comparison of 1/3 octave band of T1-turbine sound pressure level from noise emission measurements (blue), inflow-turbulence model (green) and TBL-TE model (red). All cases for a wind speed (hub height) of 8.0 m/s (6.3 m/s at 10 m height) and n = 22 rpm.

4.2.3.2 Comparing models with microphone array measurements

The microphone array measurements are compared to the models in Figure 4.16, where the experimental 1/3 octave bands and the corresponding bands from the models can be seen for positions 1-4. The experimental bands were obtained by integrating the intensities in the microphone array images. For each of the four positions, the wind speed and tip-speed ratio for that specific array recording has been implemented in the models. Overall, the inflow-turbulence model seems to fit better although for most of the bands, the measured values lies between the two models.

The directivity of both models (see Figure 4.14) results in low levels for position 1. Although the measured spectrum shows the lowest levels for position 1 (partly explained by the low wind speed during the position 1 recording), the difference compared to the other positions is smaller (apart from the 1000 Hz band). However, the uncertainty in this angle is large, due to varying wind direction and the extended range of azimuth angles over which sound is emitted. Therefore, in reality we cannot expect to see such sharp directional cancellations as predicted by the relatively simple models. Additionally, the ambient turbulence intensity was larger during the measurement at position 1 (as seen in Table 3.1). The noise produced by ambient turbulence is relevant at a wider range of blade-azimuth angles, even if the levels are

generally low. However, if the directivity factor suppresses noise due to self-generated turbulence, the noise contribution due to the ambient turbulence might also become relevant.

The measured spectra indicate spectral peaks. No peaks are present in neither of the modeled spectra. The inflow-turbulence model is based on a homogeneous spectrum of frequencies of the inflow-turbulence and the semi-empirical TBL-TE model is based on airfoil noise measurements without narrow peaks. The spectral peaks seem to roughly be harmonics of a fundamental frequency at about 750 Hz, which could be the Strouhal frequency of some characteristic length of the blade-strut attachment construction. Assuming a Strouhal number of 0.2, the corresponding length would be about 7 mm. In any case, as the blade passes through turbulence that was created within the blade-strut system just a single second ago, the turbulence spectrum is likely to be non-homogeneous.

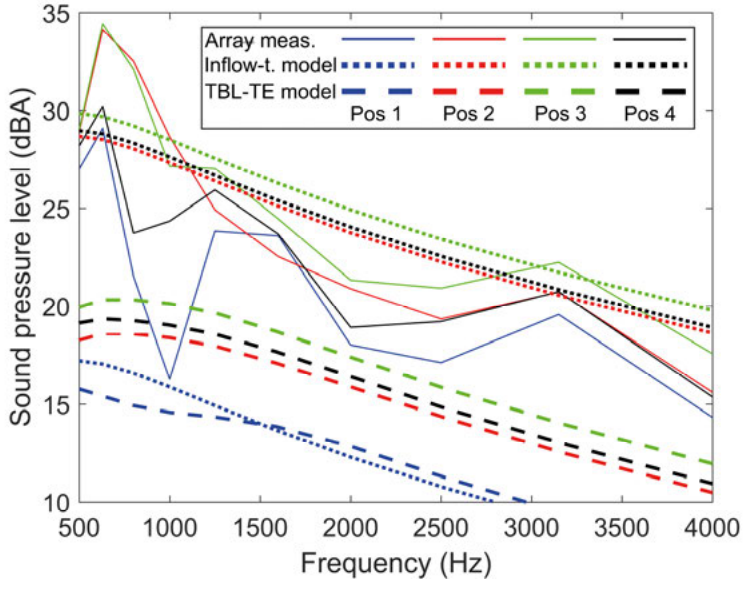

Figure 4.16: Comparison of 1/3 octave band of T1-turbine sound pressure level from inflow-turbulence model (dotted) and TBL-TE model (dashed) as well as the microphone array measurement (solid). For each position, the wind speed used for modelling was the same as during microphone array recordings (see Table 3.1).

4.2.3.3 Further discussion regarding prevailing noise source.

Both the comparison between the two models, the noise emission measurement and the microphone array measurements indicate that inflow-turbulence noise is the prevailing noise source for the T1-turbine.

Additionally, the results from "4.2.2 Microphone array measurements" suggest that it is reasonable to assume that the lower-frequency noise is due to turbulent inflow on the blade leading edge. Furthermore, the position of the lower-frequency source appears to be within the region where high turbulence can be expected,

originating predominantly from the blade-strut joint, as seen in Figure 2.1 and according to the discussion in "2.2.1.2 Inflow-turbulence noise model". The model for inflow-turbulence noise in equation (2.9) indicates a strong dependence on the local wind speed, which is indeed maximal at the observed source position. Also, the presence of the higher-frequency noise contribution at the precise position of the blade-strut joint suggests that turbulence is likely to be created there.

Consequently, it seems like the noise produced by the T1 turbine is due to turbulent inflow that is created by the turbine itself, which in turn degrades the power-conversion performance of the turbine. If it is possible to mitigate the turbulence production in the blade-strut system, this is likely to both enhance the power factor and lower the overall noise level. The development of the 500-kW Darrieus (Full-Darrieus turbine) VAWT[12] at Sandia National Laboratories during the 1980s is described in [4]. Each blade of their test-bed VAWT consisted of five pieces with different chords joined together, as it was not possible to manufacture a blade with continuously varying chord. By smoothing the joints, the maximum power factor was reported to increase from 0.41 to 0.43. Additionally, adding struts to the Full Darrieus, which was needed to maintain structural integrity for some designs, was reported to degrade performance with power levels reduced as much as 20% [4]. It is clear that the turbine performance is sensitive to adding extra structure on top of the ideal airfoil shape. Based on these considerations it would be very interesting to study the effect of changing the smoothness of the blade-strut joints of the T1 turbine, regarding both the power factor and noise emission. It appears likely that smoothing the joints would be the best way to reduce the total noise level produced by an H-rotor of this size.

4.2.3.4 Regarding the IEC standard when measuring noise emission from a VAWT

The IEC61400-11 standard implies measuring noise emission from a VAWT at a downwind distance $R_h = H + D$, which is a longer distance than the $R_h = H + D/2$ that is implied for HAWTs. This is probably the case because of the distance to the blade at its closest position will be approximately the same in both cases. However, as the most noise seem to be generated when the oncoming blade moves in the opposite wind direction and thus is at a tower distance from the downwind observer, using the same recording distance for VAWTs as for HAWTs seem to be more reasonable. Also, the indicated noise directivity with relatively low levels for the downwind position suggests that this position might not be the most proper one when measuring noise emission from VAWTs.

4.3 Eigenfrequencies of tower and guy wires

Here, the derived expressions from "2.3 Eigenfrequencies of the semi-guy-wired tower" are compared to the measurements and simulations from "3.3

[12] For more info about the specific turbine see "1.1.1 Darrieus turbines in North America (1970-80s)".

Eigenfrequency measurements and simulations" so that the validity of the expressions can be evaluated.

4.3.1 Eigenfrequency of the semi-guy-wired tower

The eigenfrequency of the semi-guy-wired tower can be calculated with the derived expression (2.24), using the effective spring force from (2.33) and effective top mass from (2.37) as well as tower properties from Table 1.2, wire properties from Table 1.3 and second moment of area from Table 2.1. To evaluate the effect of how the second moment of area is chosen (see "2.3.3.2 Second moment of area") and if the tower mass is accounted for or not (see "2.3.3.3 Incorporating tower mass"), all four combination of these choices are calculated. This way, the effect of these choices can be evaluated one by one when comparing with the corresponding simulated results in "4.3.1.1 Simulation of tower eigenfrequency". In Table 4.5, these results can be seen, where the first case (A1) uses the simplest formula for the second moment of area (a in Table 2.1) and no tower mass. In A2, the tower mass is taken into account according to expression (2.37). In A3, the conical shape and the height of guy wire fixation is taken into account (b and c in Table 2.1 for freestanding and guy-wired, respectively) when calculating the second moment of area. In A4, the measures from both A2 and A3 are combined. For all cases, the results for the freestanding tower from expression (2.15) with m_{eff} from (2.35), can also be seen in Table 4.5.

Table 4.5: *Analytical results from the simple pipe approach (A1), pipe with mass (A2), massless with conical shape and h taken in account for second moment of area (A3) and as A3 but with mass (A4).*

[Hz]	A1	A2	A3	A4
Freestanding	0.633	0.538	0.742	0.630
With Guy Wires	1.534	1.348	1.364	1.198

To verify the derived analytical expressions as well as evaluating the effect of how the second moment of area is chosen and the importance of incorporating the distributed tower mass (as discussed in "2.3.3 Effective spring constant, second moment of area and tower mass"), the analytical results are compared to g-force measurements, FEM-simulations and on-site experience of eigenfrequencies.

4.3.1.1 Simulation of tower eigenfrequency

FEM-simulations for eigenfrequencies of the tower were carried out using SolidWorks Simulation. Several models were simulated to evaluate the different options for choosing second moment of area and tower mass that are described in "2.3.3 Effective spring constant, second moment of area and tower mass".

First a much simplified 3D-model was used with a massless pipe representing the tower and a point mass at the top. The reason for this was to verify the FEM-results with the results from the analytical calculation A1. The top mass consisted of the estimated mass of the wings and struts and other parts situated at the upper part of the tower. This simulation is referred to as FEM1. A more realistic model was

then used with the tower mass included (mass from parts suspended to the tower such as the shaft, flanges, ladders etc. was compensated for by raising the density of the tower). This simulation is referred to as FEM2 and results from this model are expected to be close to that of A2. Then a massless model with the actual cone-shape of the real tower (called FEM3) was simulated. Results from this model are expected to come close to that of A3, where the shape of the tower is taken into consideration when calculating the second moment of area. Then a combination of FEM2 and FEM3 with both tower mass and conical shape was simulated. This is called FEM4 and results are expected to come close to that of A4. Finally, the model in the FEM5 simulation was similar to that of FEM4 but with part of the top mass redistributed by simple versions of wings and struts. The sum of mass is still the same but a moment of inertia will be added which will affect the turbine movement. Guy wires were then added for all five cases by simulating a spring connector with an adequate spring constant calculated from the wire properties.

Influence on the results from the main shaft in addition to its mass was neglected for all models as the shaft is only attached to the tower by bearings at the bottom and the top which, in combination with splines at the bottom and the middle, adds minimal stiffness to the tower.

Figure 4.17: The model geometry for the different FEM-simulations. From left: FEM1/2, FEM3/4, FEM5.

For all cases, adding guy wires will increase the value of the eigenfrequency which is expected since a restoring force is added to the tower. The differences between FEM1-5 are what could be expected. Additional mass will lower the eigenfrequency, guy wires present or not. The conical shape of the tower will increase the second moment of area and thereby increase the eigenfrequency. However, for the guy wire case, the frequency is lowered, probably because the second moment of area of the tower has largest effect at the height of guy wire

fixation. This because the anchoring of the guy wires will make the tower move around this point rather than the base of the tower. Finally, the distribution of mass away from the mass center in FEM5 gives a moment of inertia to the mass, which will slow down movement and lower the eigenfrequency.

Table 4.6: *Result comparison of the different FEM-simulations.*

[Hz]	FEM1	FEM2	FEM3	FEM4	FEM5
Freestanding	0.632	0.538	0.783	0.700	0.663
With Guy Wires	1.549	1.365	1.483	1.368	1.236

Figure 4.18: Maximum displacement for the first-mode eigenfrequency without guy wires (left) and with guy wires (right) for FEM5. Deformation scale 700:1.

4.3.1.2 Tower eigenfrequency g-force measurements

In Figure 4.19, a plot of the FFT from the g-force measurements can be seen and the eigenfrequency can here be read to 1.158 Hz. In [88] a similar study was performed on the T1-turbine before the guy wires were mounted, here the first-mode eigenfrequency was measured to 0.757 Hz.

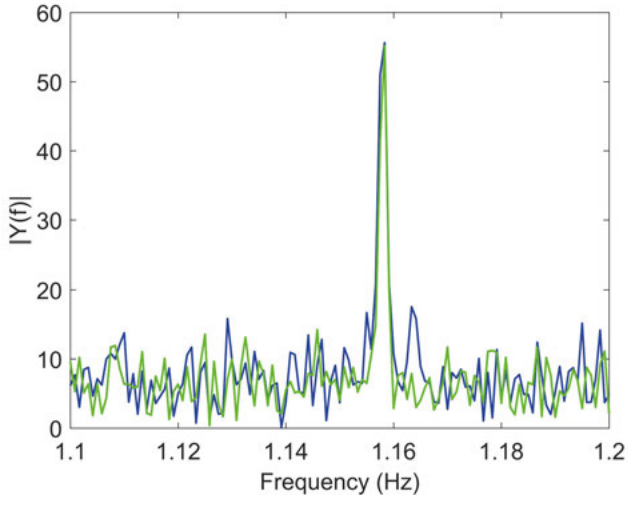

Figure 4.19: A zoomed in section of the FFT of the semi-guy-wired tower. Blue and green lines represent the x- and y-axis of the accelerometer.

4.3.1.3 On-site experience

In addition to analytical, FEM and experimental analysis, an indication of the first-mode eigenfrequency can also be attained from on-site experience of turbine behavior at different rotational speeds. Before the turbine was equipped with guy wires, resonance was shown at approximately 15 rpm, while after attaching guy wires, resonance was instead shown at 17 rpm and 23 rpm [3]. The 15 rpm and 23 rpm resonances can be assumed to originate from the tower eigenfrequency being excited by the blade-passing frequency and thus the eigenfrequencies are 0.75Hz and 1.15Hz respectively. The 17 rpm resonance can be assumed to originate from the guy wire eigenfrequency being excited by the blade-passing frequency and thus the wire eigenfrequency is 0.85 Hz.

4.3.1.4 Verifying analytical expressions

In Table 4.7, the results from the analytical and FEM models as well as for experiments and on-site observations are compared. First of all the analytical results from A1 agree very well with the corresponding FEM1-results, which is an indication that the derived analytical model is correct. The most realistic analytic result A4 seem to underestimate compared to the corresponding FEM4, especially with guy wires. Since A2 correspond much better with FEM2 than A3 do with FEM3, this is most likely due to a too simple approach for choosing second moment of area. Although approximations made in the estimation of tower and top mass, material properties and the neglecting second moment of area added by the internal structure, the FEM5 results come quite close to experimental and observational results. This is suggesting that the model simplifications in the simulation have been reasonable.

Table 4.7: *Comparison of first-mode eigenfrequency from analytical expressions with simulations, experiments and on-site observations.*

[Hz]	A1	A2	A3	A4	Exper.	Observ.
Freestanding	0.633	0.538	0.742	0.630	0.76	0.75
Guy Wires	1.534	1.348	1.364	1.198	1.16	1.15
	FEM1	FEM2	FEM3	FEM4	FEM5	
Freestanding	0.632	0.538	0.783	0.700	0.663	
Guy Wires	1.549	1.365	1.483	1.368	1.236	

There are several sources of discrepancies. Masses on top and inside the tower have been estimated as have some of the material properties. Effects upon the second moment of area from the main shaft and other structures on the inside of the tower have been neglected. Vertical effects from the guy wires as well as effects from the wires "hanging down" have also been neglected. With these simplifications and generalizations in mind the results from the FEM5 simulation lies well within the error margin. The analytical results confirm with the FEM-results with the same simplifications, although slightly underestimating the result for most cases. Consequently, the derived analytical expression can confidently be used to indicate the magnitude of change in eigenfrequency when modifying a tower or guy-wire property.

4.3.2 Eigenfrequency of guy wire

On site behavior has shown a resonance occurring at 17 rpm that likely originates from the guy wires (see section "4.3.1.3 On-site experience"). Using equation (2.25), the current pre-tension can be estimated to 83 kN, which together with equations (2.24), (2.26), (2.29) as well as tower and guy-wire properties gives the Campbell diagram for the current setup which can be seen in Figure 4.20. If using guy wires, it is desirable to keep them resonance free. This can be done by letting the lower limit of the wire frequency range lie above the 3P load at nominal rotational speed (see Figure 4.20).

Altering the guy-wire eigenfrequency can be done by changing the pre-tension, using a wire with different properties (μ and E_wA) or changing wire attachment (h, L and α). By combining equations (2.26), (2.29) and the relations between E_wA, k and $\tilde{k}$, a diagram can be produced (Figure 4.21) showing which E_wA and pre-tension combinations that keeps the wire resonance free for different inclination angles. This diagram is hereafter referred to as an EA-T diagram. As an approximation, for a given wire model[13], the linear density μ is set to vary linearly with the axial stiffness E_wA. The wire length L is set to vary with the inclination angle α, but the height of guy-wire attachment h is kept constant since a high guy-wire attachment is desirable, and a certain clearance to the turbine blades is required.

[13] Same material and design but for different diameters, looking at a product sheet there is a small difference between the E_wA - μ ratio for different wire diameters, this difference is small and deemed as reasonable to neglect.

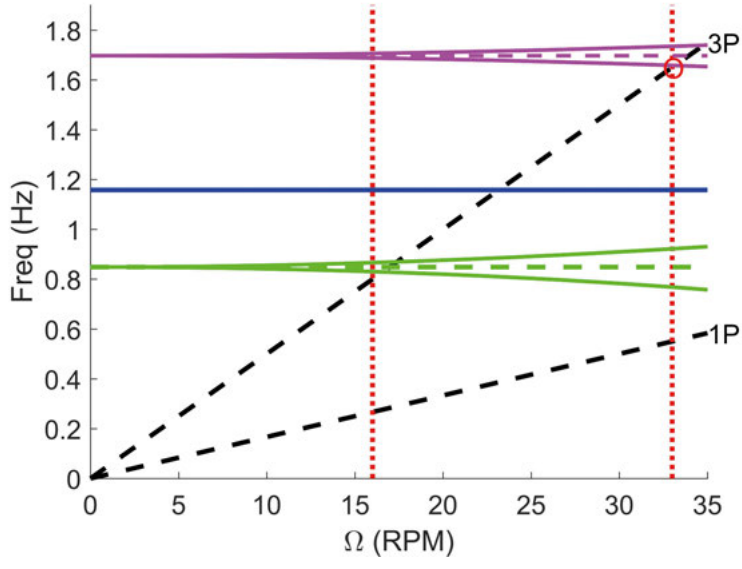

Figure 4.20: Campbell diagram for the T1-turbine with current setup of 83-kN wire pre-tension (blue: tower frequency, green: wire frequency). The figure also shows a resonance-free guy wire which implies a pre-tension of 334 kN (magenta).

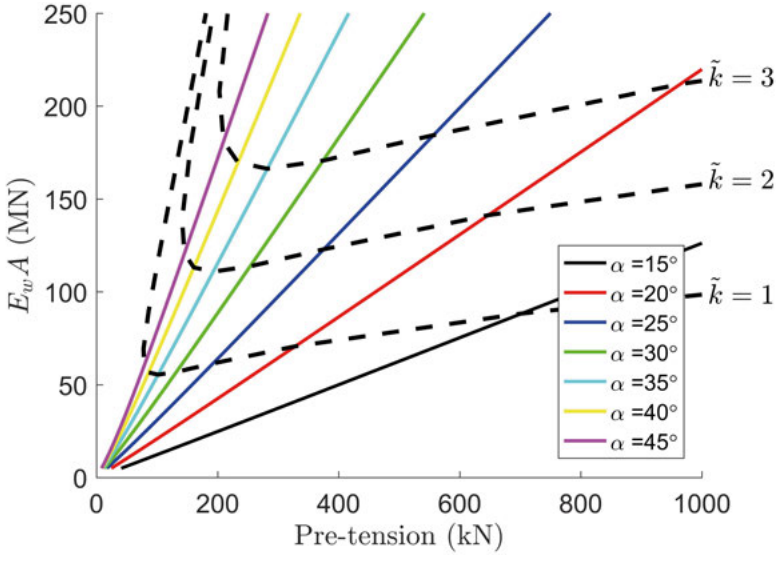

Figure 4.21: EA-T diagram showing which combination of E_wA, pre-tension and α that is needed for achieving a certain $\tilde{k}$ (MN/m) as well as a resonance-free wire. Right side of the inclination angle line gives an eigenfrequency >3P.

The effective spring force $\tilde{k}$, which represents the effect on the tower, can also be seen in the EA-T diagram, allowing comparing different resonance-free options. As an example, the current guy-wire setup with $\alpha = 27.2°$ and $E_wA = 124$ MN, which gives an effective spring force $\tilde{k} = 2.10$ MN/m, requires a pre-tension of 334 kN to stay resonance free. Using the diagram, it can be seen that the same $\tilde{k}$ can be achieved with a less land consuming inclination angle $\alpha = 40°$, a slightly lighter wire with $E_wA \approx 115$MN, as well as a remarkably lower pre-tension of 167 kN. The EA-T diagram is an illustrative tool for choosing wire setup for a pre-defined effective spring force. The diagram can in a similar way be retrieved and used for larger VAWTs as well as other guy-wired structures that have a given upper limit for eigenfrequency excitement by the dynamic loads.

5. Conclusions

In this thesis a vertical-axis wind turbine has been examined, by experiments as well as analytical work and simulations. The 200-kW H-rotor VAWT, in this work referred to as the T1-turbine, has been the main research subject although most results can be generalized to suit a typical H-rotor. Below, you will find a summary of the main conclusions.

The influence from turbulence on the wind energy extraction for the T1-turbine is studied by evaluating 1030 hours of logged operational data and using the measure turbulence intensity (TI). As the standard power curve is elevated with turbulence due to the cubic effect, a power to wind cube plot is used, allowing comparing the turbine's real performance for different turbulence intensities. The following main conclusions can be drawn:

- The T1-turbine has seemingly good ability to extract wind energy at turbulent conditions, indicating an advantage in energy extraction at turbulent sites for VAWTs compared to HAWTs
- There is a clear influence from turbulence on $\lambda_{C_{p-max}}$ for the T1-turbine. Seemingly, $\lambda_{C_{p-max}}$ increases with TI, giving an opportunity to tune the control strategy of the turbine to enhance the total efficiency of the turbine.
- Also for the T1-turbine, a maximum $C_p = 0.33$ was found at $\lambda = 4.3$.

The noise characteristics of the T1-turbine are studied by two separate noise measurement campaigns: a noise emission measurement to evaluate the noise levels and a microphone array measurement aiming to localize aerodynamic noise sources. The measurements are compared to models of the deemed two most likely aerodynamic noise mechanisms: turbulent-boundary-layer trailing-edge noise (TBL-TE) and inflow-turbulence noise. The main conclusions are:

- The noise emission of the T1-turbine was measured to 94.1 dBA at 6 m/s 10 m above ground which is at the absolute lower range compared to similar size HAWTs. At 8 m/s, the noise emission was measured to 96.2 dBA, however, at this wind speed the turbine was not run at target tip speed and thus stalling. The effect of this upon the noise level is unclear as there are two balancing effects.

- The microphone array measurements shows that most noise is produced when the blade is travelling in the opposite wind direction. Results from the measurements also lead to the indication that most noise is due to inflow-turbulence on the blade leading edge, where the turbulence is likely to be created during the previous blade-strut-system passage.
- After comparing results from the noise emission and the microphone array measurements with models of TBL-TE and inflow-turbulence noise respectively, it is suggested that the inflow-turbulence noise is the prevailing noise mechanism.

The eigenfrequencies of the T1-turbine's semi-guy-wired tower are also studied. Analytical expressions describing the first-mode eigenfrequency of both tower and guy wire has been derived and verified by experiments and simulations. The expressions can be used as:

- The derived analytical expression (2.24), found on page 40, can be used to give an indication of the magnitude of change in eigenfrequency when modifying a tower or guy-wire property. The effective spring force $\tilde{k}$ and the effective top mass m_{eff} (replacing m) used in the expression can be retrieved from (2.33) and (2.37) respectively.
- Likewise, expression (2.29) found on page 42, can, when inserted in (2.26) be used to find the approximate range of eigenfrequencies for all three wires for a given wind speed.

6. Summary of papers and author contribution

This chapter contains a summary of all papers included in this thesis and the author's contribution to each paper.

Paper I

Turbulence influence on wind energy extraction for a medium size vertical axis wind turbine

Logged data from a period of 14 month with the T1-turbine operating in wind speeds up to 9 m/s are analyzed and the relation between power performance and turbulence intensity is studied. This is done with two different approaches. One approach is in line with the IEC standard which allows comparing results with other standardized power curves. The second approach allows isolating the effect of the turbulence from the cubic variation of power with wind speed and thus getting a better view of the performance under turbulence. The results are compared to available similar results for HAWTs. Furthermore, the data is also used to create a $C_p(\lambda)$-curve which is compared to a curve simulated by a double multiple streamtube model.

The paper is published in *Wind Energy, Volume 19* (2016).

The author has written the paper and done the majority of the work including evaluating the logged data. The simulation with the double multiple streamtube model was done by Anders Goude.

Paper II

Turbulence influence on optimum tip speed ratio for a 200 kW vertical axis wind turbine

Logged data from a period of 14 month (the same data as in paper I) with the T1-turbine operating in wind speeds up to 9 m/s are analyzed and the relation between optimum tip-speed ratio and turbulence intensity is studied. This is done by dividing 10 min mean values in different turbulence intensity ranges and producing multiple $C_p(\lambda)$ curves.

The paper is published in *Journal of Physics: Conference series*, Volume 753, article no. 032048, 2016. The paper was presented with a poster at The Science of making Torque from Wind (TORQUE 2016) conference in Munich, Germany.

The author has written the paper and done the majority of the work including evaluating the logged data.

Paper III

Noise emission of a 200 kW Vertical Axis Wind Turbine

Noise measurements similar to that described by IEC61400-11, the international standard for deciding noise emissions from wind turbines, are performed on the T1-turbine. Furthermore, the results have been compared to a semi-empirical model for turbulent-boundary-layer trailing-edge (TBL-TE) noise. When comparing the experimental results with accessible noise emission statements of similar size HAWTs, the T1-turbine is found to have a noise emission at the absolute bottom of the range. The experimental results are also compared to the semi-empirical model and conclusions are drawn regarding the origin of the noise.

The paper is published in *Energies, Volume 9, Issue 1* (2016).

The author has evaluated the measurement data and written most of the paper. The comparison between experimental results and the semi-empirical model was done together with Fredric Ottermo who was responsible for setting up the model. The measurements were performed by consultant company ÅF Infrastructure.

Paper IV

Location of aerodynamic noise sources from a 200-kW vertical-axis wind turbine

Measurements using a microphone array, a.k.a. a noise camera, are performed on the T1-turbine with the aim to locate the origin of the aerodynamic noise sources. Furthermore, the results have been compared to a semi-empirical model for inflow-turbulence noise which ads further to the knowledge of the origin of the aerodynamic noise drawn from Paper III. The results show that most noise is generated where turbulence from the passage of the previous blade is known to be present. This together with the fact that the semi-empirical model produces noise levels of the correct order of magnitude indicates that inflow-turbulence noise is more important than TBL-TE noise for this type of VAWT.

The paper is re-submitted after revision to Journal of Sound and Vibration.

The author has taken part in both performing and analyzing the measurements as well as written a part of the paper. Fredric Ottermo has written most of the paper and was responsible for setting up the model. Anders Nordborg was responsible for the most vital parts of the measurement analysis.

Paper V

Eigenfrequencies of a vertical axis wind turbine tower made of laminated wood and the effect upon attaching guy wires

An analytical model describing the first-mode eigenfrequency of a semi-guy-wired vertical-axis wind turbine tower is derived. The model is evaluated using FEM-simulations as well as experimental g-force measurements on the T1-turbine. The model is found to be useful for estimating the eigenfrequency when adding guy wires or altering guy-wire setup for a tower firmly attached to the ground.

The paper is published in *Wind Engineering, Volume 38, no 3* (2014).

The author has written the paper and done the majority of the work including taking part in the analytical derivations which Fredric Ottermo was main responsible for.

Paper VI

Avoidance of resonances in a semi-guy-wired vertical axis wind turbine

The analytical model from Paper V is modified to an expression of how the first-mode eigenfrequency of a guy wire is affected by wind load. A range growing with wind speed and containing the eigenfrequencies of all three guy wires is created. The expression is evaluated by FEM-simulations and a diagram is created (here called EA-T diagram) showing how to combine wire size, inclination angle and pre-tension for a resonance-free wire with a certain effective spring force acting on the tower.

The paper was presented with a poster at the *EWEA 2014 Annual Event* in Barcelona and is published as a reviewed conference paper in its proceedings.

The author has written the paper and done the majority of the work including design of the EA-T diagram. The analytical work was made together with Fredric Ottermo who was the main responsible for this part.

Paper VII

Noise propagation from a vertical axis wind turbine

Initial noise measurements are performed on the T1-turbine and a similar size HAWT. Multiple recording units are placed in line downwind of the turbines to investigate and compare noise propagation. The frequency distribution of the noise is also analyzed and compared. Results indicate lower relative levels for frequencies below 3000 Hz, especially within 600-1200 Hz, for the T1-turbine as well as a more rapid noise decline, possibly explained by the lower levels at low frequencies.

The paper was presented oraly at the *inter.noise2014 conference* in Melbourne and is published as a reviewed conference paper in its proceedings.

The author has written the paper and done the majority of the work. Measurements performed together with Sebastian Larsson.

7. Summary in Swedish (Sammanfattning på svenska)

Vertikalaxlade vindkraftverk (VAWTs) har en historia som sträcker sig tillbaka till 1000-talets Persien vilket gör dem äldre än de typiska vindkvarnarna som dök upp i Europa på 1300-talet. Gällande elgenererande och nätanslutna vindkraftverk har dock de vertikalaxlade vindkraftverken haft betydligt mindre framgång än de idag vanliga och kommersiellt gångbara horisontalaxlade vindkraftverken (HAWTs), som haft en märkbar teknisk utveckling sedan inte minst 1980-talet. Men de vertikalaxlade vindkraftverken har flera fördelar som ändå gör de intressanta för framtiden: generator och andra vitala delar kan placeras på marknivå vilket förenklar service samt möjliggör en design som fokuserar på kostnadseffektivitet snarare än vikt och volymminimering. Det har dessutom argumenterats att vertikalaxlade vindkraftverk har lägre ljudemission än motsvarande horisontalaxlade, att deras fysiska egenskaper passar bättre för både uppskalning (>10MW) och för placering på flytande offshoreplattformar.

Arbetet som denna avhandling utgörs av är utfört i ett sammarbete mellan Högskolan i Halmstad och Uppsala Universitet. Ett 200 kW semi-stagat vertikalaxlat vindkraftverk av typen H-rotor, som ägs av Uppsala Universitet men är lokaliserat i Falkenberg nära Halmstad, har varit det huvudsakliga forskningsobjektet även om resultaten kan generaliseras för en typiskt H-rotor. Grunden till avhandlingen utgörs av sju vetenskapliga artiklar där undertecknad varit huvud- eller medförfattare. Avhandlingen kan delas in i tre delar som tar upp olika fysikaliska aspekter hos vertikalaxlade vindkraftverk: (1) hur turbulens påverkar vindenergialstringen, (2) hur det aerodynamiska ljudet uppstår och (3) det semi-stagade tornets egenfrekvenser. Dessa delar beskrivs i korthet nedan.

Turbulensens påverkan på vindenergialstringen har undersökts genom att anlysera 1030 timmar av loggad driftsdata med hjälp av storheten turbulensintensitet (TI). Då vindens energiinnehåll för en given medelvind är länkad till turbulensen, så har både vanliga vind-effektkurvor och vindkub-effektkurvor använts i analysen. Turbulensens påverkan på kurvorna i sig samt påverkan på optimalt löptal har studerats för att utvärdera vindkraftverkets egenskaper under olika turbulensförhållanden. När resultaten jämförs med liknande resultat för horisontalaxlade vindkraftverk så påvisas goda egenskaper för att ta upp de energirika turbulenta vindbyarna vilket i sin tur indikerar att turbintypen troligtvis passar för turbulenta siter. Mer turbulens visar sig också ge ett högre optimalt löptal – en vetskap som kan användas för att göra kontrollstrategin mer effektiv. Analysen

visade också att vindkraftverkets maximala C_p för normala turbulensförhållanden var 0.33 och hittas vid ett löptal $\lambda = 4.3$.

Ljudalstringen har studerats med dels en mer traditionell ljudemissionsmätning för att utvärdera ljudnivån och dels en ljudkameramätning för att kunna lokalisera ljudkällorna. Dessa ljudmätningar har sedan jämförts med modeller för de två mest troliga mekanismerna för aerodynamiskt ljud från vindkraftverk. Resultaten indikerar att så kallat ”inflow-turbulence noise”, dvs ljud som uppstår när uppströmsturbulens interagerar med vingens framkant, är den viktigaste ljudmekanismen för vertikalaxlade vindkraftverk. Dessutom har ljudemissionen för vindkraftverket mäts upp till 94.1 dBA och 96.2 dBA för 6 respektive 8 m/s (vindhastighet 10 m ovan mark), vilket är lågt i jämförelse med horisontalaxlade vindkraftverk av motsvarande storlek. Ljudkameramätningarna visade att mest ljud skapas när vingen rör sig i motsatt vindriktning och därmed utsätts för turbulens skapad av föregående blad och bärarm.

Vindkraftverkets unika tornlösning (beskrivs som semi-stagat) gör att det inte finns något färdig utryck att använda gällande tornets egenfrekvens. Det semi-stagade tornets egenfrekvenser har därför studerats och analytiska uttryck för första böjmodens egenfrekvens för både det semi-stagade tornet och själva stagvajern har tagits fram. Dessa utryck har sedan verifierats med simuleringar och mätningar.

References

[1] A. P. Schaffarczyk, *Understanding Wind Power Technology - Theory, Deployment and Optimisation*. Wiley, 2014.

[2] S. Eriksson, H. Bernhoff, and M. Leijon, "Evaluation of different turbine concepts for wind power," *Renewable and Sustainable Energy Reviews,* vol. 12, no. 5, pp. 1419-1434, 2008.

[3] J. Kjellin, "Vertical Axis Wind Turbines: Electrical System and Experimental Results," Ph.D. thesis, Uppsala University, 2012.

[4] H. J. Sutherland, D. E. Berg, and T. D. Ashwill, "A retrospective of VAWT technology," *Sandia National Laboratories,* 2012.

[5] F. Ottermo and H. Bernhoff, "An upper size of vertical axis wind turbines," *Wind Energy,* vol. 17, no. 10, pp. 1623-1629, 2013.

[6] M. Borg, A. Shires, and M. Collu, "Offshore floating vertical axis wind turbines, dynamics modelling state of the art. Part I: aerodynamics," *Renewable and Sustainable Energy Reviews,* vol. 39, pp. 1214-1225, 2014.

[7] J. F. Manwell, J. G. McGowan, and A. L. Rogers, *Wind Energy Explained: Theory, Design and Application*. Wiley, 2010.

[8] T. Ackermann and L. Söder, "An overview of wind energy-status 2002," *Renewable and Sustainable Energy Reviews,* vol. 6, no. 1–2, pp. 67-127, 2002.

[9] G. J. M. Darrieus, "Turbine having its rotating shaft transverse to the flow of the current," Patent Patent no. 1835018, 1931.

[10] I. Paraschivoiu, *Wind turbine design: with emphasis on Darrieus concept*. Presses inter Polytechnique, 2002.

[11] A. W. E. Association, "Vertical axis wind turbine: the history of the DOE program," *US Department of Energy, Sandia National Laboratories, American Wind Energy Association,* 1986.

[12] S. Tudor, "A Brief History of Wind Power Development in Canada 1960s-1990s," http://www.uoguelph.ca/engineering/sites/default/files/resources_History%20Canada.pdf (2016-10-21), 2010.

[13] S. Peace, "Another approach to wind," *Mechanical Engineering,* vol. 126, no. 6, pp. 28-31, 2004.

[14] P. Gipe, *Wind Energy for the Rest of Us: A Comprehensive Guide to Wind Power and How to Use It*. Bakersfield, California: Wind-Works.Org, 2016.

[15] A. P. Schaffarczyk, *Introduction to wind turbine aerodynamics*. Springer, 2014.

[16] I. D. Mays, C. A. Morgan, M. B. Anderson, and S. J. R. Powles. The 500 kW VAWT 850 is now operating. *Modern Power Systems (October issue, 1990)*.

[17] T. J. Price, "UK large-scale wind power programme from 1970 to 1990: the Carmarthen Bay experiments and the musgrove vertical-axis turbines," *Wind Engineering,* vol. 30, no. 3, pp. 225-242, 2006.

[18] "Technical sheet: Construction and Demonstration of 5 Vertical Axis Wind Turbines H-Rotor with 300 kW Rated Power," Heidelberg Motor GmbH, http://cordis.europa.eu/opet/fiches/rwe-8.htm (2016-10-19), 1998.

[19] "Wind Energy Converter H-rotor - Product guide," Heidelberg Motor GmbH, 1993.

[20] T. Tin *et al.*, "Energy efficiency and renewable energy under extreme conditions: Case studies from Antarctica," *Renewable Energy,* vol. 35, no. 8, pp. 1715-1723, 2010.

[21] J. Ribrant and L. Bertling, "Survey of failures in wind power systems with focus on Swedish wind power plants during 1997-2005," in *2007 IEEE Power Engineering Society General Meeting*, Tampa, USA, 2007.

[22] S. Apelfröjd, S. Eriksson, and H. Bernhoff, "A Review of Research on Large Scale Modern Vertical Axis Wind Turbines at Uppsala University," *Energies,* vol. 9, no. 7, p. 570, 2016.

[23] U. S. Paulsen *et al.*, "DeepWind-from idea to 5 MW concept," *Energy Procedia,* vol. 53, pp. 23-33, 2014.

[24] W. Tjiu, T. Marnoto, S. Mat, M. H. Ruslan, and K. Sopian, "Darrieus vertical axis wind turbine for power generation II: Challenges in HAWT and the opportunity of multi-megawatt Darrieus VAWT development," *Renewable Energy,* vol. 75, pp. 560-571, 2015.

[25] "ANew Institute website, "http://www.anew-institute.com/" (2016-11-06)," 2016.

[26] H. Riegler, "HAWT versus VAWT: Small VAWTs find a clear niche," *Refocus,* vol. 4, no. 4, pp. 44-46, 2003.

[27] D. Ehrnberg, "Offshore energy storage device," Patent Patent no. US20120114486 A1, 2012.

[28] S. Eriksson, "Direct driven generators for vertical axis wind turbines," Ph.D. thesis, Uppsala University, 2008.

[29] P. Deglaire, "Analytical aerodynamic simulation tools for vertical axis wind turbines," Ph.D. thesis, Uppsala University, 2010.

[30] A. Goude, "Fluid Mechanics of Vertical Axis Turbines: Simulations and Model Development," Ph.D. thesis, Uppsala University, 2012.

[31] F. Bülow, "A generator perspective on vertical axis wind turbines," Ph.D. thesis, Uppsala University, 2013.

[32] E. Dyachuk, "Aerodynamics of Vertical Axis Wind Turbines: Development of Simulation Tools and Experiments," Ph.D. thesis, Uppsala University, 2015.

[33] J. Olauson, "Modelling Wind Power for Grid Integration Studies," Ph.D. thesis, Uppsala University, 2016.

[34] S. Apelfröjd, "Grid Connection of Permanent Magnet Generator Based Renewable Energy Systems," Ph.D. thesis, Uppsala University, 2016.

[35] S. Sjökvist, "Demagnetization and Fault Simulations of Permanent Magnet Generators," PhD. thesis, Uppsala University, 2016.

[36] M. Rossander, "Blade force measurements and electrical torque ripple of a vertical axis wind turbine," Licentiate thesis, Uppsala University, 2016.

[37] P. Eklund, "Rare Earth Metal-Free Permanent Magnet Generators," Licentiate thesis, Uppsala University, 2016.

[38] V. A. Riziotis and S. G. Voutsinas, "Fatigue loads on wind turbines of different control strategies operating in complex terrain," *Journal of Wind Engineering and Industrial Aerodynamics,* vol. 85, no. 3, pp. 211-240, 2000.

[39] W. D. Lubitz, "Impact of ambient turbulence on performance of a small wind turbine," *Renewable Energy,* vol. 61, pp. 69-73, 2014.

[40] A. Honrubia, A. Vigueras-Rodríguez, and E. Gómez-Lázaro, "The Influence of Turbulence and Vertical Wind Profile in Wind Turbine Power Curve," in *Progress in Turbulence and Wind Energy IV*: Springer, 2012, pp. 251-254.

[41] K. Kaiser, W. Langreder, H. Hohlen, and J. Højstrup, "Turbulence correction for power curves," in *Wind Energy*: Springer, 2007, pp. 159-162.

[42] R. Wagner, M. Courtney, T. J. Larsen, and U. Schmidt Paulsen, "Simulation of shear and turbulence impact on wind turbine performance," Danmarks Tekniske Universitet, Risø Nationallaboratoriet for Bæredygtig Energi, 2010.

[43] J. Gottschall and J. Peinke, "How to improve the estimation of power curves for wind turbines," *Environmental Research Letters,* vol. 3, no. 1, p. 015005, 2008.

[44] T. Bertényi, C. Wickins, and S. McIntosh, "Enhanced energy capture through gust-tracking in the urban wind environment," in *48th AIAA Aerospace Sciences Meeting Including the New Horizons Forum and Aerospace Exposition*, Orlando, USA, 2010, p. 1376.

[45] H. K. Versteeg and W. Malalasekera, *An introduction to computational fluid dynamics: the finite volume method*. Pearson Education, 2007.

[46] S. Yahaya and J. Frangi, "Cup anemometer response to the wind turbulence-measurement of the horizontal wind variance," *Annales Geophysicae,* vol. 22, no. 10, pp. 3363-3374, 2004.

[47] S. Wharton and J. K. Lundquist, "Atmospheric stability affects wind turbine power collection," *Environmental Research Letters,* vol. 7, no. 1, p. 014005, 2012.

[48] D. Bowdler and H. G. Leventhall, *Wind Turbine Noise*. Multi Science Publishing Company, Limited, 2011.

[49] E. Adolfsson, "Riktvärden för ljud från vindkraft," Swedish Environmental Protection Agency, 2010.

[50] K. Bolin, "Wind Turbine Noise and Natural Sounds: Masking, Propagation and Modeling," Ph.D. thesis, Royal Institute of Technology, 2009.

[51] E. Pedersen, "Human response to wind turbine noise: Perception, annoyance and moderating factors," Ph.D. thesis, The Sahlgrenska Academy, University of Gothenburg, 2007.

[52] S. Oerlemans, P. Sijtsma, and B. Méndez López, "Location and quantification of noise sources on a wind turbine," *Journal of Sound and Vibration,* vol. 299, no. 4–5, pp. 869-883, 2007.

[53] C. Pearson, "Vertical axis wind turbine acoustics," Ph.D. thesis, Cambridge University, 2014.

[54] A. Iida, A. Mizuno, and K. Fukudome, "Numerical simulation of aerodynamic noise radiated from vertical axis wind turbines," in *Proceedings of the 18 International Congress on Acoustics*, Kyoto, Japan 2004.

[55] H. Dumitrescu, V. Cardos, A. Dumitrache, and F. Frunzulica, "Low-frequency noise prediction of vertical axis wind turbines," *Proceedings of the Romanian Academy,* vol. 11, no. 1, pp. 47-54, 2010.

[56] T. F. Brooks, D. S. Pope, and M. A. Marcolini, *Airfoil self-noise and prediction*. National Aeronautics and Space Administration, Office of Management, Scientific and Technical Information Division, 1989.

[57] G. Tescione, D. Ragni, C. He, C. S. Ferreira, and G. Van Bussel, "Near wake flow analysis of a vertical axis wind turbine by stereoscopic particle image velocimetry," *Renewable Energy,* vol. 70, pp. 47-61, 2014.

[58] P. Moriarty and P. G. Migliore, *Semi-empirical aeroacoustic noise prediction code for wind turbines*. National Renewable Energy Laboratory, 2003.

[59] M. V. Lowson, "Assessment and prediction of wind turbine noise," Flow Solutions Ltd., 1993.

[60] R. Amiet, "Acoustic radiation from an airfoil in a turbulent stream," *Journal of Sound and vibration,* vol. 41, no. 4, pp. 407-420, 1975.

[61] S. Buck, S. Oerlemans, and S. Palo, "Experimental validation of a wind turbine turbulent inflow noise prediction code," in *22nd AIAA/CEAS Aeroacoustics Conference*, Lyon, France, 2016, p. 2953.

[62] W. Tjiu, T. Marnoto, S. Mat, M. H. Ruslan, and K. Sopian, "Darrieus vertical axis wind turbine for power generation I: Assessment of Darrieus VAWT configurations," *Renewable Energy,* vol. 75, pp. 50-67, 2015.

[63] *IEC 61400-11: Wind turbine generator systems–Part 11: Acoustic noise measurement techniques, Edition 3*, 2012.

[64] T. F. Brooks and W. M. Humphreys, "A deconvolution approach for the mapping of acoustic sources (DAMAS) determined from phased microphone arrays," *Journal of Sound and Vibration,* vol. 294, no. 4, pp. 856-879, 2006.

[65] P. Sijtsma, "Acoustic beamforming for the ranking of aircraft noise," National Aerospace Laboratory Report No. NLR-TP-2012-137, 2012.

[66] H. D. Young and R. A. Freedman, *Sears and Zemansky's University physics: With modern physics*. Pearson Addison Wesley. ISBN: 0321501314, 9780321501318.

[67] F. Ottermo and H. Bernhoff, "Resonances and aerodynamic damping of a vertical axis wind turbine," *Wind Engineering,* vol. 36, no. 3, pp. 297-304, 2012.

[68] S. Eriksson and H. Bernhoff, "Generator-damped torsional vibrations of a vertical axis wind turbine," *Wind Engineering,* vol. 29, no. 5, pp. 449-461, 2005.

[69] T. G. Carne, "Guy cable design and damping for vertical axis wind turbines," in "SAND80-2669, Sandia National Laboratories, Albuquerque, New Mexico, USA," Report, Sandia National Laboratories, Albuquerque, USA, 1980.

[70] T. G. Carne, "Guy Cable and Foundation Design Techniques," in *Vertical Axis Wind Turbine (VAWT) Design Technology Seminar for Industry*, Albuquerque, USA, 1980: Sandia National Laboratories.

[71] R. D. Blevins, *Formulas for natural frequency and mode shape*. Malabar, USA: Krieger publishing company, 2001, p. 492.

[72] C. Norling and J. Österman, "Physics Handbook for Science and Engineering," *Studentlitteratur, Lund, Sweden,* 2002.

[73] C. J. Wong and M. D. Miller, *Guidelines for Electrical Transmission Line Structural Loading* (no. 74). ASCE Publications, 2010.

[74] F. P. Beer, *Vector Mechanics for Engineers: Statics and dynamics*. McGraw-Hill Companies, 2010.

[75] *IEC 61400-12-1: Wind turbines part 12-1: Power performance measurements of electricity producing wind turbines, Edition 1.*, 2005.

[76] R. Wagner, I. Antoniou, S. M. Pedersen, M. S. Courtney, and H. E. Jørgensen, "The influence of the wind speed profile on wind turbine performance measurements," *Wind Energy,* vol. 12, no. 4, pp. 348-362, 2009.

[77] S. Eriksson, H. Bernhoff, and M. Leijon, "A 225 kW direct driven PM generator adapted to a vertical axis wind turbine," *Advances in Power Electronics,* vol. 2011, 2011.

[78] *IEC 61672-1 Electroacoustics - Sound level meters - Part 1: Specifications, Edition 2*, 2013.

[79] Z. Prime and C. Doolan, "A comparison of popular beamforming arrays," in *ACOUSTICS 2013*, Victor Harbor, Australia, 2013.

[80] "Acoular - Acoustic testing and source mapping software ", ed. http://www.acoular.org/, (2016-08-15).

[81] E. Sarradj and G. Herold, "Acoular - Open-Source-Software zur Anwendung von Mikrofonarrayverfahren," presented at the DAGA 2016, Aachen, Germany, 2016.

[82] J. Kjellin, F. Bülow, S. Eriksson, P. Deglaire, M. Leijon, and H. Bernhoff, "Power coefficient measurement on a 12 kW straight bladed vertical axis wind turbine," *Renewable energy,* vol. 36, no. 11, pp. 3050-3053, 2011.

[83] A. Goude and F. Bülow, "Robust VAWT control system evaluation by coupled aerodynamic and electrical simulations," *Renewable energy,* vol. 59, pp. 193-201, 2013.

[84] "Noise measurement of VESTAS V27-225kW Wind Turbine," DNV Det Norske Veritas, http://www.southhams.gov.uk/planningdocs/1/00/20/23/00202341.pdf (2014-06-27), 1995.

[85] "GEV MP-R32 m rotor diameter sound power levels," VERGNET Wind Turbines, http://www.cesa.org/assets/2013-Files/ITAC/VergnetGEVMPRacousticreport.pdf (2014-07-23), 2013.

[86] "Noise assessment NORWIN 29 225 kW wind turbine," 24Acoustics, http://planning.allerdale.gov.uk/portal/servlets/AttachmentShowServlet?ImageName=218119 (2014-07-23), 2012.

[87] "General Noise Specifications WTN 250 kW," Wind Technik Nord GmbH, http://www.newport.gov.uk/stellent/groups/public/documents/planningdocument/cont616474.pdf (2014-07-23), 2012.

[88] M. D'Ambrosio and M. Medaglia, "Vertical Axis Wind Turbines: History, Technology and Applications," Master Thesis, Halmstad University, 2010.

Acta Universitatis Upsaliensis

Digital Comprehensive Summaries of Uppsala Dissertations from the Faculty of Science and Technology 1485

Editor: The Dean of the Faculty of Science and Technology

A doctoral dissertation from the Faculty of Science and Technology, Uppsala University, is usually a summary of a number of papers. A few copies of the complete dissertation are kept at major Swedish research libraries, while the summary alone is distributed internationally through the series Digital Comprehensive Summaries of Uppsala Dissertations from the Faculty of Science and Technology. (Prior to January, 2005, the series was published under the title "Comprehensive Summaries of Uppsala Dissertations from the Faculty of Science and Technology".)

Distribution: publications.uu.se
urn:nbn:se:uu:diva-316385

ACTA
UNIVERSITATIS
UPSALIENSIS
UPPSALA
2017